CHARACTERIZATION OF CONDUCTION PROCESSES IN AMORPHOUS SEMICONDUCTORS

J. L. Stone

Texas A and M Research Foundation

Prepared for:

Advanced Research Projects Agency

31 August 1972

a report

from the Texas A&M
RESEARCH FOUNDATION
College Station, Texas

110

Final Technical Report

ARPA Order Number - 1562

Grant Number - DA-ARO-D-31-124-71-G49

Program Code Number - 0D10

Principal Investigator - Dr. J. L. Stone
(713) 845-7441

Name of Grantee - Texas A&M Research Foundation

Project Scientist - (See Principal Investigator)

Effective Date of Grant - January 1, 1971

Title of Work - Characterization of Conduction Processes in Amorphous Semiconductors

Grant Expiration Date - August 31, 1972

Amount of Grant - $50,015.00

Sponsored by

Advanced Research Projects Agency
ARPA Order No. 1562

APPROVED FOR PUBLIC RELEASE:
DISTRIBUTION UNLIMITED

I

ABSTRACT

In many semiconductor materials, the photodielectric effect is manifested as a decrease in the real part of the complex dielectirc constant. This is due to a phase shift in the velocity of the ionized carriers interacting with a high frequency electric field. The optically induced dielectric perturbation is used to vary the resonant frequency of a microwave cavity.

Amorphous semiconductors are known to possess various levels of trapping centers, and it can be shown that the magnitude of the photodielectric effect is proportional to the density and levels of these traps. Both a fast and a slow decay of photoconductivity (a change in the imaginary part of the complex dielectric constant) are known to exist. The initial rapid decay is attributed to the capture of carriers by the high density of traps below the mobility edges of the conduction band. The long relaxation time is due to the slow decay towards equilibrium through the processes of hopping and capture of carriers by deep traps.

Several different samples of $2As_2Se_3$, As_2Te_3, As_2Se_3, As_2Se_3, As_2S_3 and Si(3%) Ge(4%) As(38%) Te(55%) were used in the photodielectric tests. However, none of the experiments, conducted at room temperature, 77°K, or 4.2°K, produced any photodielectric effect. Several reasons for the absence of positive results were analyzed, and it was decided that low optical absorption of the material, low mobility of free carriers, and short momentum relaxation time were the reasons which best explained the negative photodielectric tests.

The thermally stimulated conductivity experiment provides a convenient way to investigate these hypotheses by investigating the trapping centers existing in the material under study. Analysis for the discrete case is

well documented in the literature, and a theoretical derivation is presented to extend the analysis to the quasi-continuous case.

Samples of amorphous thin film As_2Se_3 were investigated in this manner. The material was found to undergo an irreversible transformation at 385°K with a band gap of 1.35 eV before the transformation and 1.71 eV afterwards. The untransformed material was found to possess a discrete trapping level at 0.843 eV with a density of 9.73×10^{14} cm^{-3}. The thermal velocity of the carriers was 6.34×10^{6} cm/sec, and the capture cross section was 2.7×10^{-18} cm^2. These results indicate that the Mott-Davis model is more applicable to amorphous As_2Se_3 than the CFO model.

TABLE OF CONTENTS

CHAPTER

LIST OF FIGURES

INTRODUCTION

The following final technical report is divided into two sections. These sections correspond to the major efforts expended in examining the conduction processes in amorphous semiconductors.

The photodielectric tests established that relaxation times are on the order of 10^{-15} sec., or relaxation approximately every lattice spacing. Hence, a low mobility is observed. All technical details are examined in detail in Part I.

The results of thermally stimulated conductivity tests (TSC) show a definite relationship to the Mott-Davis Model. A density of states is noted at 0.843 eV which places them just below the half-gap energy. The states behave as acceptors in agreement with p-type conductivity noted from thermal power measurements. The detail of the TSC experiments are presented in Part II.

The graduate student participants and degrees earned are as follows:

1.) S. A. Collins - Master of Science - Electrical Engineering

2.) J. D. Bryant - Master of Science - Electrical Engineering

3.) A. K. Malholtra - Thesis in progress

4.) W. C. Wang - Master of Engineering

5.) J. G. Weatherwax - Dropped from school, personal reasons

Two papers were presented at the Fourth International Conference on Amorphous and Liquid Semiconductors, Ann Arbor. The papers were published in the Journal of Noncrystalline Solids, Volume 8-10 as follows:

"Identification of Trapping Mechanisms in Amorphous Compounds Using Cavity Perturbation Techniques", Page 614-620.

"Minor Switching and RF Oscillations in Amorphous Semiconductors", Page 432-438.

Other papers are in preparation and copies will be forwarded as soon as they are completed.

PART I

CHAPTER I

THE PHOTODIELECTRIC EFFECT

1.1 Introduction

The conductivity of semiconductors lies between that of good conductors and good insulators and is determined in part by temperature and free carrier density. At liquid helium temperature (4.2°K) an intrinsic semiconductor sample can be described as an insulator except for the fact that the valence band electrons are bound much less tightly than those of a good insulator. This provides the possibility that one or more electrons can gain enough thermal energy to move into the conduction band.

In well established material properties studies Arndt, Hartwig and Stone[1]) and Hartwig and Hinds[2]) have shown that the complex conductivity of semiconductors can be effectively changed by photon-induced free carrier creation. Irradiation of a semiconductor sample with light of quantum energy, hv, greater than the ionization energy produces free carriers at the expense of bound charges. These free carriers, created as electron-hole pairs, add to the conductivity of the material for a length of time determined by the created carrier lifetime.

The photodielectric effect is a decrease in the real part of the

complex dielectric constant as explained by Stone[3]). This decrease results from a phase shift in the velocity of the free carriers interacting with the microwave electric field. This can be characterized by a complex conductivity or mobility.

1.2 Cavity Perturbation

A method of measuring small changes in the dielectric constant of a material is to use such changes in the material to perturb the inherent field patterns of a resonant cavity. According to cavity perturbation theory, when the sample is excited by light photons, a change in the dielectric constant of the material will effect a change in the cavity Q and resonant frequency.

The complex angular frequency for a resonant cavity is

$$\omega = \omega_r + j\omega_i \qquad (1.1)$$

where

ω_r = real component

ω_i = imaginary component

Sucher and Fox[4]) derive the following equation for the frequency perturbation, $\frac{\delta\omega}{\omega_2}$, of a resonant cavity.

$$\frac{\delta\omega}{\omega_2} = \frac{\omega_2-\omega_1}{\omega_2} \approx \frac{f_{r_2}-f_{r_1}}{fr_2} + j\left(\frac{1}{2Q_2} - \frac{1}{2Q_1}\right) \qquad (1.2)$$

In this equation the subscript "1" denotes the cavity loaded with an unexcited sample and the subscript "2" denotes the cavity loaded with the sample after excitation. Thus, through the above equation, it

can be seen that cavity perturbation contains both a change in the resonant frequency and a change in the cavity Q.

Stone[3]) takes the dot product of Maxwell's equations

$$\begin{aligned} \bar{\nabla} \times \bar{E} &= -j\omega\mu\bar{H} \\ \bar{\nabla} \times \bar{H} &= j\omega\epsilon\bar{E} \end{aligned} \tag{1.3}$$

and integrates over the volume of the cavity, V_c, to show the relative frequency change due to dielectric samples to be

$$\frac{\omega_1-\omega_0}{\omega_1} = \frac{\Delta\omega_1}{\omega_1} = \frac{\int_{V_c}(\epsilon_0-\epsilon_1)\bar{E}_0\cdot\bar{E}_1 dV - \int_{V_c}(\mu_0-\mu_1)\bar{H}_0\cdot\bar{H}_1 dV}{\int_{V_c}(\epsilon_0\bar{E}_0\cdot\bar{E}_1-\mu_0\bar{H}_0\cdot\bar{H}_1)dV} \tag{1.4}$$

$$\frac{\omega_2-\omega_0}{\omega_2} = \frac{\Delta\omega_2}{\omega_2} = \frac{\int_{V_c}(\epsilon_0-\epsilon_2)\bar{E}_0\cdot\bar{E}_2 dV - \int_{V_c}(\mu_0-\mu_2)\bar{H}_0\cdot\bar{H}_2 dV}{\int_{V_c}(\epsilon_0\bar{E}_0\cdot\bar{E}_2-\mu_0\bar{H}_0\cdot\bar{H}_2)dV} \tag{1.5}$$

where the subscript "0" denotes the cavity with no sample, the subscript "1" denotes the cavity with an unexcited dielectric sample and subscript "2" denotes the cavity with the sample excited by light. Equations (1.4) and (1.5) are the general perturbation equations that describe a change in resonant cavity frequency. Frequency shifts caused by exciting the sample with light are considered as perturbations on the original perturbations caused by loading the cavity with the sample. The assumptions made in the derivation of the above equations are that the sample volume, V_s, is

much smaller than the cavity volume, V_c, and that in the cavity, $\mu_0=\mu_1=\mu_2$ and $\varepsilon_0=\varepsilon_1=\varepsilon_2$ everywhere except in the sample.

If the sample is placed in a position of maximum electric field and minimum magnetic field and with its surface perpendicular to the electric field then another assumption, that the sample does not perturb the electric fields in the cavity, can be made. With this assumption the electric flux densities can be set equal.

$$D_0 = D_1 = D_2 \tag{1.6}$$

$$\varepsilon_0\bar{E}_0 = \varepsilon_1\bar{E}_1 = \varepsilon_2\bar{E}_2 \tag{1.7}$$

Therefore, $\mu_1=\mu_2=\mu_0$ is the sample and the perturbation equations (1.4) and (1.5) can be written as

$$\frac{\Delta\omega_1}{\omega_1} \simeq \frac{\frac{\varepsilon_0-\varepsilon_1}{\varepsilon_1}\int_{V_s} 2\varepsilon_0 |E_{0_{rms}}|^2 dV}{\int_{V_c}(\varepsilon_0\bar{E}_0\cdot\bar{E}_1-\mu_0\bar{H}_0\cdot\bar{H}_1)dV} \tag{1.8}$$

$$\frac{\Delta\omega_1}{\omega_1} \simeq \frac{\frac{\varepsilon_0-\varepsilon_2}{\varepsilon_2}\int_{V_s} 2\varepsilon_0 |E_{0_{rms}}|^2 dV}{\int_{V_c}(\varepsilon_0\bar{E}_0\cdot\bar{E}_2-\mu_0\bar{H}_0\cdot\bar{H}_2)dV} \tag{1.9}$$

The integrals in the right side of equations (1.8) and (1.9) are similar in that they are ratios of energy stored in the sample to that stored in the cavity. These ratios are not easily calculated because they require the knowledge of the E fields at various points in space but may be experimentally determined as a

geometric filling factor. This factor is a constant for a fixed sample size and is denoted as G. Thus equations (1.8) and (1.9) become

$$\frac{\Delta\omega_1}{\omega_1} \simeq -\frac{\varepsilon_0-\varepsilon_1}{\varepsilon_1} G_1 \qquad (1.10)$$

$$\frac{\Delta\omega_2}{\omega_2} \simeq \frac{\varepsilon_0-\varepsilon_2}{\varepsilon_2} G_2 \qquad (1.11)$$

In the integral over the volume of the cavity, it is assumed that the dielectric constant of the material is such that the fields are undisturbed. Thus $\bar{E}_0=\bar{E}_1=\bar{E}_2$ and $\bar{H}_0=\bar{H}_1=\bar{H}_2$ and therefore $G_0=G_1=G_2=G$.

$$G = \frac{\int_{Vs} 2\varepsilon_0 |E_{0_{rms}}|^2 dV}{\int_{Vc} (\varepsilon_0 \bar{E}_0^2 - \mu_0 \bar{H}_0^2) dV}$$

$$= \frac{2\int_{Vs} \varepsilon_0 |E_{0_{rms}}|^2 dV}{\int_{Vc} (\varepsilon_0 |E_0|^2 + \mu_0 |H_0|^2) dV}$$

$$= \frac{\int_{Vs} \varepsilon_0 |E_{0_{rms}}|^2 dV}{2\int_{Vc} \varepsilon_0 |E_{0_{rms}}|^2 dV} \qquad (1.12)$$

(Since electric fields are assumed real quantities, magnetic fields are imaginary and $\varepsilon_0|E_0|^2=\mu_0|H_0|^2$.)

The change in resonant frequency that occurs when the sample is excited is

$$\frac{\delta\omega}{\omega} \simeq \frac{\Delta\omega_2}{\omega_2} - \frac{\Delta\omega_1}{\omega_1} \qquad (1.13)$$

Substituting from equations (1.10) and (1.11)

$$\frac{\delta\omega}{\omega} = \varepsilon_0 G\left[\frac{1}{\varepsilon_2} - \frac{1}{\varepsilon_1}\right] \qquad (1.14)$$

Arndt[5]) developed the relationship between the complex dielectric constant $\varepsilon^* = \varepsilon_0(\varepsilon' - j\varepsilon'')$ and the physical properties of semiconductors in order to predict the frequency and Q perturbations. Using a classical free carrier treatment, the differential equation relating the forces on a carrier in a semiconductor subjected to a periodic field can be written:

$$m^* \frac{dV}{dt} + \frac{m^*V}{\tau} = eEe^{j\omega t} \qquad (1.15)$$

where

E = the magnitude of the electric field

$m^* \frac{dV}{dt}$ = accelerating force

m^* = effective mass of the carrier

V = velocity of the carrier

$\frac{m^*}{\tau}$ = friction force

τ = momentum relaxation time

ω = driving angular frequency

e = charge of the carrier

The above equation is obtained from the relation F=ma=qE with the addition of a retarding friction force due to momentum. This equation is solved[5]) for the carrier velocity and then an expression

for the complex conductivity is written as

$$\sigma = \frac{ne^2}{m^*}\left[\frac{\tau}{1+\omega^2\tau^2} - j\frac{\omega\tau^2}{1+\omega^2\tau^2}\right] \qquad (1.16)$$

where n is the concentration of optically created free carriers.

The complex dielectric constant can be expressed as

$$\varepsilon^* = \varepsilon + \frac{\sigma}{j\omega} = \varepsilon_0(\varepsilon_\ell + \frac{\sigma}{j\omega\varepsilon_0}) = \varepsilon_0(\varepsilon' - j\varepsilon'') \qquad (1.17)$$

where

ε' = real part of the dielectric constant

ε'' = imaginary part of the dielectric constant

ε_ℓ = lattice contribution to the dielectric constant

Substituting equation (1.16) into (1.17), the result is

$$\varepsilon^* = \varepsilon_0(\varepsilon_\ell - \frac{ne^2}{m^*\varepsilon_0}\frac{\tau^2}{1+\omega^2\tau^2} + \frac{ne^2}{j\omega\varepsilon_0 m^*}\frac{\tau}{1+\omega^2\tau^2}) \qquad (1.18)$$

with real and imaginary parts:

$$\varepsilon' = \varepsilon_\ell - \frac{ne^2}{m^*\varepsilon_0}\frac{\tau^2}{1+\omega^2\tau^2}$$

$$\varepsilon'' = \frac{ne^2}{m^*\varepsilon_0}\frac{\tau}{1+\omega^2\tau^2} \qquad (1.19)$$

Thus the dielectric constant of a semiconductor decreases when the conduction electron density is increased due to photon-induced contributions.

Now the dielectric constants can be expressed as

$$\frac{\varepsilon_2}{\varepsilon_0} = (\varepsilon_\ell - kn) - j(\frac{kn}{\omega\tau})$$

$$\frac{\varepsilon_2}{\varepsilon_0} = (\varepsilon_\ell - \varepsilon_\psi) - j\left(\frac{\varepsilon_\psi}{\omega\tau}\right) \tag{1.20}$$

and

$$\frac{\varepsilon_1}{\varepsilon_0} = \varepsilon_\ell \tag{1.21}$$

where

$$k = \frac{e^2}{m^*\varepsilon_0} \frac{\tau^2}{1+(\omega\tau)^2} \tag{1.22}$$

and

$$\varepsilon_\psi = kn$$

$$n = \frac{\alpha P_\psi \tau_L}{h\nu V_s} \tag{1.23}$$

= number of optically created free carriers

α = conversion efficiency

P_ψ = incident light power

τ_L = free carrier lifetime

h = Planck's Constant

ν = frequency of incident light

V_s = volume of sample subject to created free carrier density

Equation (1.20) expresses the dielectric constant as the difference of the lattice contributions and photon-induced contributions. Thermal contributions are neglected since the work will be done in liquid helium (4.2°K).

Substituting equations (1.20) and (1.21) into equation (1.14) results in

$$\frac{\delta\omega}{\omega} = G\left[\frac{\varepsilon_\ell - \varepsilon_\psi + j\varepsilon_\psi/\omega\tau}{(\varepsilon_\ell - \varepsilon_\psi)^2 + (\varepsilon\psi/\omega\tau)^2} - \frac{1}{\varepsilon_\ell}\right] \qquad (1.24)$$

Referring to equation (1.2), the real part of equation (1.24) is related to the frequency shift of the cavity. Therefore

$$\mathrm{Re}\left(\frac{\delta\omega}{\omega}\right) = G\left[\frac{\varepsilon_\ell - \varepsilon_\psi}{(\varepsilon_\ell - \varepsilon_\psi)^2 + (\varepsilon_\psi/\omega\tau)^2} - \frac{1}{\varepsilon_\ell}\right] \qquad (1.25)$$

Equation (1.25) has been used[5]) successfully to predict the free carrier behavior of the photodielectric effect in Si, Ge, GaAs, InAs, and InSb.

1.3 Traps and Recombination Centers

Once free carriers have been created they remain free until captured at an imperfection in the material. Generally, these capturing centers are classified into two groups: (1) trapping centers - if the probability of the carrier being re-excited is greater than that of it recombining with a carrier of opposite sign (2) recombination centers - if recombination is more probable than re-excitation.

1.4 Effects of Traps

Bube[6]) discusses three principal hypotheses to explain the photodielectric effect. (1) It is another method of measuring the photoconductivity of the material. (2) It is a real change in the

dielectric constant of the material, caused by the existence of polarizable centers consisting of electrons loosely bound to traps. (3) It is a real change in the dielectric constant, but is caused by the existence of space charges at material grain boundaries.

Hinds[7]) points out that the magnitude of the photodielectric effect in CdS is directly related to the density and location of traps in the forbidden band. The first free carriers created are captured by both hole and electron traps. Soon, however, the electron traps are filled and all the electrons generated subsequently move into the conduction band. This continues until all the hole traps also become full and any holes generated are free for recombination. Figure I-1 shows the expected conduction result. During the first portion (t_0-t_1) both hole and electron traps are filling and no conduction occurs. From t_1 to t_2 conduction increases when the electron traps are filled and electrons are collected in the conduction band. At $t=t_2$ the hole traps begin to saturate and carriers generated are free for recombination.

In a very complete discussion relating to the complex dielectric constant to semiconductor properties Hinds[7]) shows that the presence of traps has a distinct influence on the relative dielectric constant. This is done by adding a term, expressing an elastic binding force, to the previously discussed equation of force on free carriers.

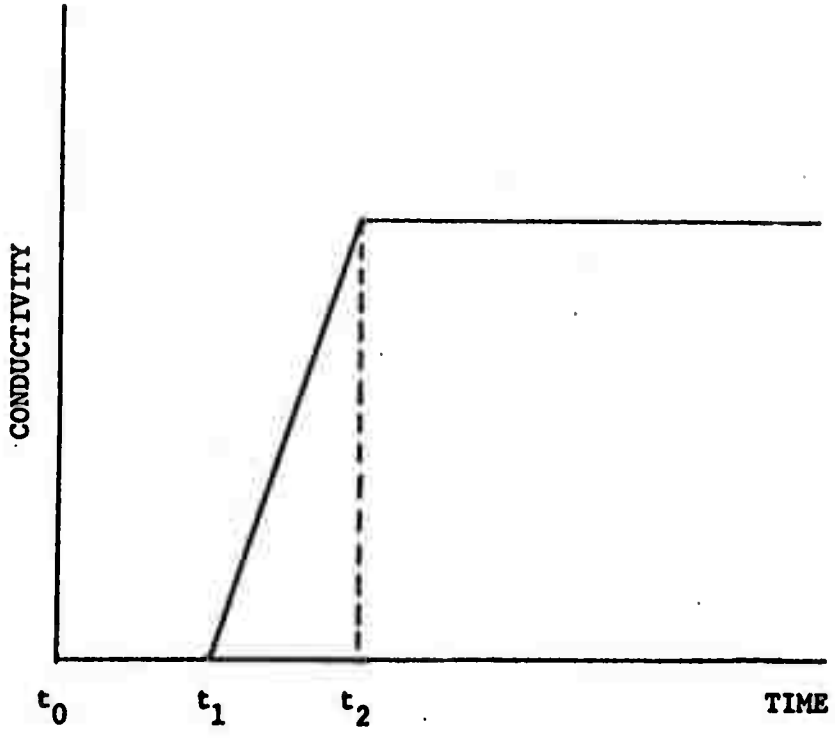

Fig. I-1 Curve of Conductivity vs Time Using Constant Light

Equation (1.15), with this binding force added, becomes

$$m^*\frac{d^2x}{dt^2} + \frac{m^*}{\tau}\frac{dx}{dt} + kx = eEe^{j\omega t} \qquad (1.26)$$

where

k = effective spring constant of the bound charge

$Ee^{j\omega t}$ = the electric field around the sample

m^* = the effective mass of the carrier

x = the displacement, in one direction, of the particle from equilibrium

τ = the momentum relaxation time

e = the charge of the carrier

The first term represents the acceleration force, the second gives the viscous damping force and the third is the elastic binding force.

Equation (1.26) is of the form required for a harmonic oscillator of frequency $\omega_0 = \sqrt{k/m^*}$. The solution of this equation is

$$x = \frac{eEe^{j\omega t}}{m^*}\,\frac{(\omega_0^2 - \omega^2 - j\omega/\tau)}{(\omega_0^2 - \omega^2)^2 + (\omega/\tau)^2} \qquad (1.27)$$

By considering surface charge densities it can be shown[7] that the relative dielectric constant is expressed as:

$$\epsilon_r = \frac{1}{\epsilon_0 Ee^{j\omega t}} \sum_i e_i x_i + 1 \qquad (1.28)$$

where

x_i = the displacement in one direction, of the partical from equilibrium

e_i = charge of the carrier

Substituting equation (1.27) into (1.28) the relative dielectric constant becomes

$$\varepsilon_r = \sum_i \frac{e_i^2}{m^*_i \varepsilon_0} \left[\frac{\omega_0^2-\omega^2-j\omega/\tau}{(\omega_0^2-\omega^2)^2+(\omega/\tau)^2}\right]_i + 1 \qquad (1.29)$$

In order to simplify equation (1.29) several assumptions are made. Only the charges which effect the dielectric perturbation due to light are considered and all others are dropped from the summation. Therefore only a few electrons, having the same mass m_i^* and charge e_i, need to be considered and these terms are taken outside the sum. The remaining electrons which do remain inside the summation can be classified into selective groups such as free, captured in deep traps, or in shallow traps. These groups are represented by a new index J and $\Delta\varepsilon_r$ is written

$$\Delta\varepsilon_r = \frac{e^2}{m^*\varepsilon_0} \sum_J \Delta n_J \left[\frac{\omega_0^2-\omega^2-j\omega/\tau}{(\omega_0^2-\omega^2)^2+(\omega/\tau)^2}\right]_J \qquad (1.30)$$

where Δn_J represents the net change in the density of electrons in the J-th group. Writing equation (1.30) in real and imaginary parts.

$$\Delta\varepsilon_r = \Delta\varepsilon_r' - j\Delta\varepsilon_r''$$

and

$$\Delta\varepsilon_r' = \frac{e^2}{m^*\varepsilon_0} \sum_J \Delta n_J \left[\frac{\omega_0^2-\omega^2}{(\omega_0^2-\omega^2)^2+(\omega/\tau)^2}\right]_J \qquad (1.31)$$

$$\Delta\varepsilon_r'' = \frac{e^3}{m^*\varepsilon_0} \sum_J \Delta n_J \left[\frac{\omega/\tau}{(\omega_0^2-\omega^2)^2+(\omega/\tau)^2}\right]_J \qquad (1.32)$$

Again considering the classical oscillator it can be shown that

$$\omega_0^2 = 1.70\text{x}10^{29}\left(\frac{m}{m^*}\right)E^3(\text{eV}) \qquad (1.33)$$

where E(eV) is the binding energy expressed in electron-volts. Based upon equations (1.31) and (1.33) the relation of E and $\Delta\varepsilon_r'$ can be noted. For a constant ω, different simplifications of $\Delta\varepsilon_r'$ can be obtained as the binding energy is varied. When $\omega_0 >> \omega$, the bracketed term in equation (1.31) may be replaced by $(1/\omega_0)^2$ and thus $\Delta\varepsilon_r'$ increases as E decreases. Now let $(\omega/\tau) > \omega_0^2$, $\Delta\varepsilon_r'$ decreases as E decreases and

$$\Delta\varepsilon_r' \propto \left[\frac{\omega_0^2}{(\omega/\tau)^2}\right] \qquad (1.34)$$

As $(\omega_0^2-\omega^2)$ changes from positive to negative, $\Delta\varepsilon_r'$ becomes zero and then negative and may be expressed as

$$\Delta\varepsilon_r' \propto \left[\frac{\omega_0^2-\omega^2}{(\omega/\tau)^2}\right] \qquad (1.35)$$

Finally when $\omega >> \omega_0$, ε_r' remains negative and the bound electron takes on the characteristics of a free carrier. For this case the equation is identical to that obtained earlier for free electrons.

$$\Delta\epsilon_r' = -\frac{ne^2}{m^*\epsilon_0}\frac{\tau^2}{1+\omega^2\tau^2} \qquad (1.36)$$

1.5 Traps in Amorphous Semiconductors

In the previous sections it is pointed out that in many materials the photodielectric effect has been exhibited due to the presence of traps. Therefore it is suspected that various amorphous semiconductors should also show some photodielectric effect since the models that have been hypothesized place many trapping sites in the forbidden band.

Cohen[8]) has applied the effects of trapping sites to the amorphous semiconductor model developed by Cohen, Fritzsche and Ovshinsky[9]). Andriesh and Kolomiets[10]) report the presence of current carrier trapping centers in the forbidden band of the amorphous semiconductor $Tl_2Se \cdot As_2Te_3$. Also multiple trapping levels are reported in the amorphous chalcogenide alloy As(50%)-Te(30%)-Ge(11%)-Si(9%) by Botila and Vancu[11]). Kolomiets, Lyubin and Averjanov[12]) describe the existence of both trapping sites and recombination centers in As_2Se_3.

Fagen and Fritzsche[13]) explain the band model for covalent amorphous alloys which was proposed by Cohen, Fritzsche, and Ovshinsky[9]). The important characteristics are a high density of localized states, shown in figure I-2 as tails from either band, and mobility edges E_v and E_c separating the localized and extended states of the conduction and valence bands, respectively. These

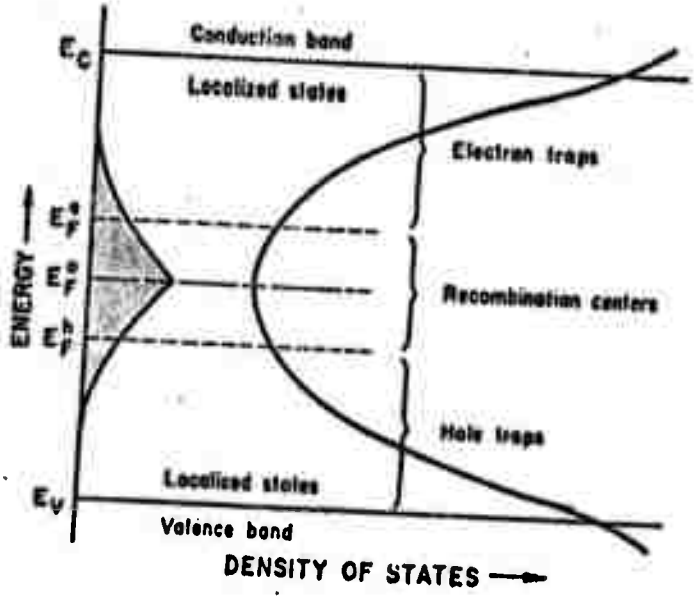

Fig. I-2 Band Model for Amorphous Alloys (ref. 13)

tails overlap near the center of the mobility gap and cause electron hopping from upper valence band states to lower conduction band states. During steady-state irradation, E_F^0 splits into electron and hole quasi-Fermi levels, E_F^e and E_F^h. When the energy source is removed, the photon-excited carriers may recombine through the recombination centers located between the electron and hole quasi-Fermi levels. This accounts for the fast component of decay of photoconductivity that has been reported[9]). During this fast decay, the quasi-Fermi levels move partly back toward equilibrium. The slow component of decay of photoconductivity, that is reported with the fast decay, suggests a relaxation process of phonon assisted tunneling between spatially separated localized states.

CHAPTER II

EQUIPMENT AND EXPERIMENTAL TECHNIQUES

Many of the experimental techniques associated with the observation of the photodielectric effect in an x-band resonant cavity have not previously been established in the Physical Electronics Laboratory. Therefore methods of material processing of amorphous compounds, use of cryogenic techniques and operation of microwave equipment will be discussed fully.

2.1 Amorphous Material Processing

The amorphous compound $2As_2Se_3 \cdot As_2Te_3$ is made in a specially designed oven in the Amorphous Semiconductor Laboratory. This oven is housed in an airtight enclosure to avoid contamination of the room by a possible explosion of the ampoule containing poisonous material. A rocking motor is also attached to the furnace in order to mix the constituents while the material is molten.

The material was made by combining two binaries, As_2Se_3 and As_2Te_3, in the desired proportions. The correct amount of each of these was weighed on an analytical balance and then loaded into a vycor tube. This was then evacuated and sealed using an oxy-hydrogen torch. The sealed ampoule was then inserted into the oven (preheated to 800°C) and allowed to remain for 8 hours. During the last hour in the oven the sample was agitated by rocking to assure a uniform mixture of all components. At the end of the 8 hour period the ampoule was removed and allowed to quinch slowly at room temperature. The sample

hardened into a solid ingot which was extracted by breaking the glass capsule.

2.2 Sample Preparation

In order to obtain a sample for use in the photodielectric measurements, the ingot was sawed into wafers approximately 2 mm thick using a jewlers saw. A fine grit sandpaper was used to lap the surfaces smooth. In order to attach the prepared sample to the teflon holder several adhesives were tried but Duro epoxy cement was found to be the most satisfactory.

2.3 The Cryogenic System

The dewar system. In order to maintain a cryogenic environment, the dewar system shown in figure II-1 is used. The evacuated envelope serves as a divider between the outer dewar containing liquid nitrogen and the inner dewar containing liquid helium.

The circuit, a resonant cavity, is suspended at the end of the stainless steel waveguide and is aligned with the lenses in both the inner and outer dewar. The light is introduced through a small hole in the cavity via these lenses. The plate which holds the waveguide rigid in the dewar can be unbolted from the header assembly to allow easy removal of the waveguide and cavity. The "O" ring seal around the header opening and a mica strip in the waveguide joint provide vacuum tight seals.

Pre-cooling procedure. In order to cool the dewars and the circuit properly, a systematic method must be followed. The dewars must

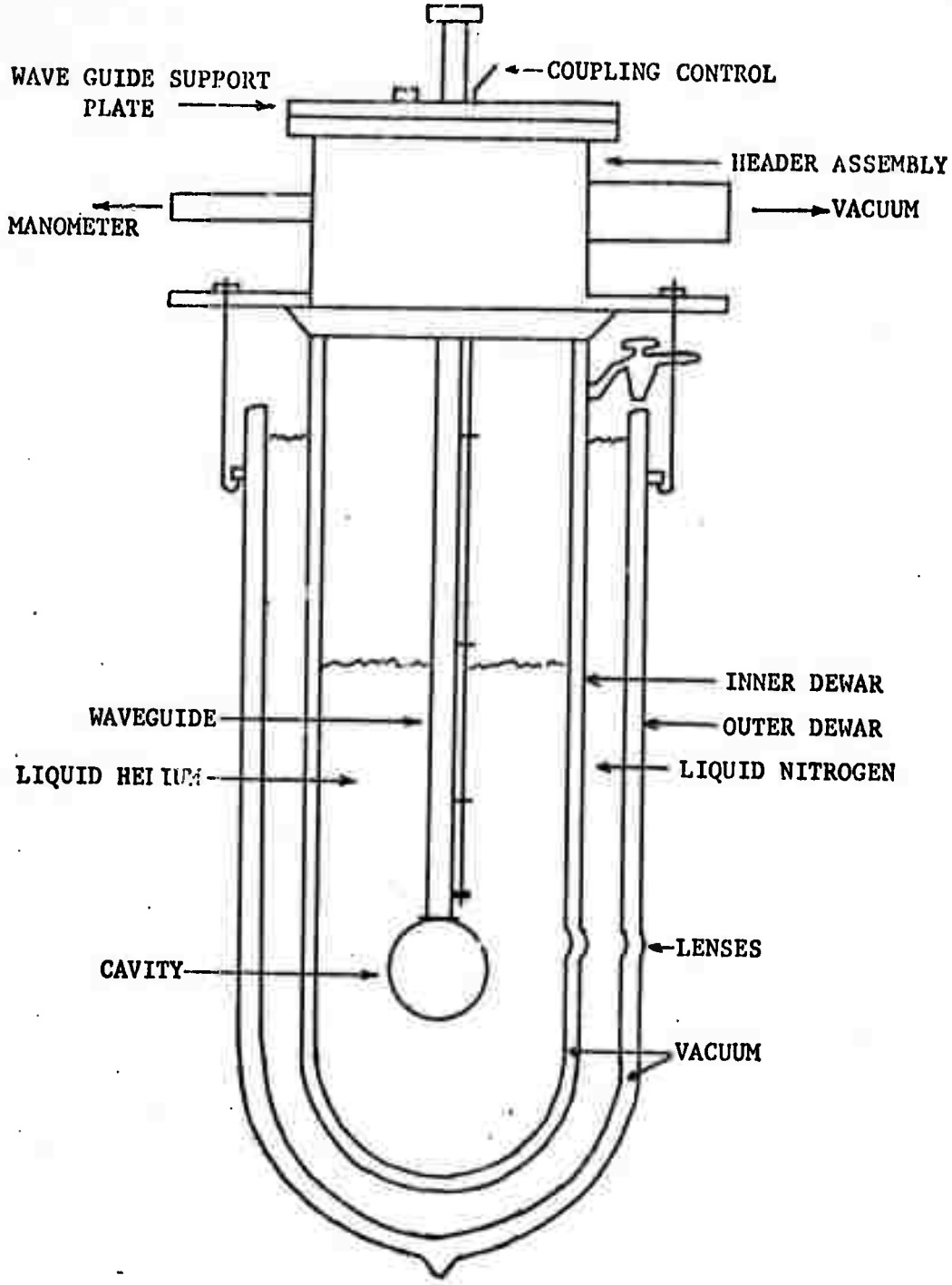

Fig. II-1 Dewar System

be clean and completely dry before the procedure is begun. First the envelope of the inner dewar must be pumped out completely in order to prevent ice from thermally shorting the liquid helium to the ambient. Next the inner dewar is evacuated and held until it is time to transfer liquid helium. Liquid nitrogen is now transfered into the outer dewar to start the cooling process and is allowed to stand for approximately eight hours. This period allows the inner dewar and the circuit it contains to cool approximately to liquid nitrogen temperature (77°K). The vacuum on the inner dewar should be removed by pressurizing it to room pressure with helium gas. Care must be used to prevent any air to enter the dewar during this stage of the procedure. Liquid helium* is then transfered by standard techniques.

2.4 Microwave Equipment

Many different pieces of microwave apparatus were integrated into the system, used as a tool to examine the amorphous compound. Figure II-2 shows the arrangement of the complete system.

Resonant Cavity. A TE-011 cylindrical cavity is used to house the sample. The currents in this mode are circular in the end plates thus no current crosses a mechanical joint. This preserves the inherent high Q of the cavity. Also the TE-011 mode produces zero electric field everywhere on the surface, therefore the coupling from the

---

*For reference, liquid helium can be obtained from Mr. Frank Fisher (713)944-3160, Houston, Texas or Linde Corporation (806)376-4295, Amarillo, Texas.

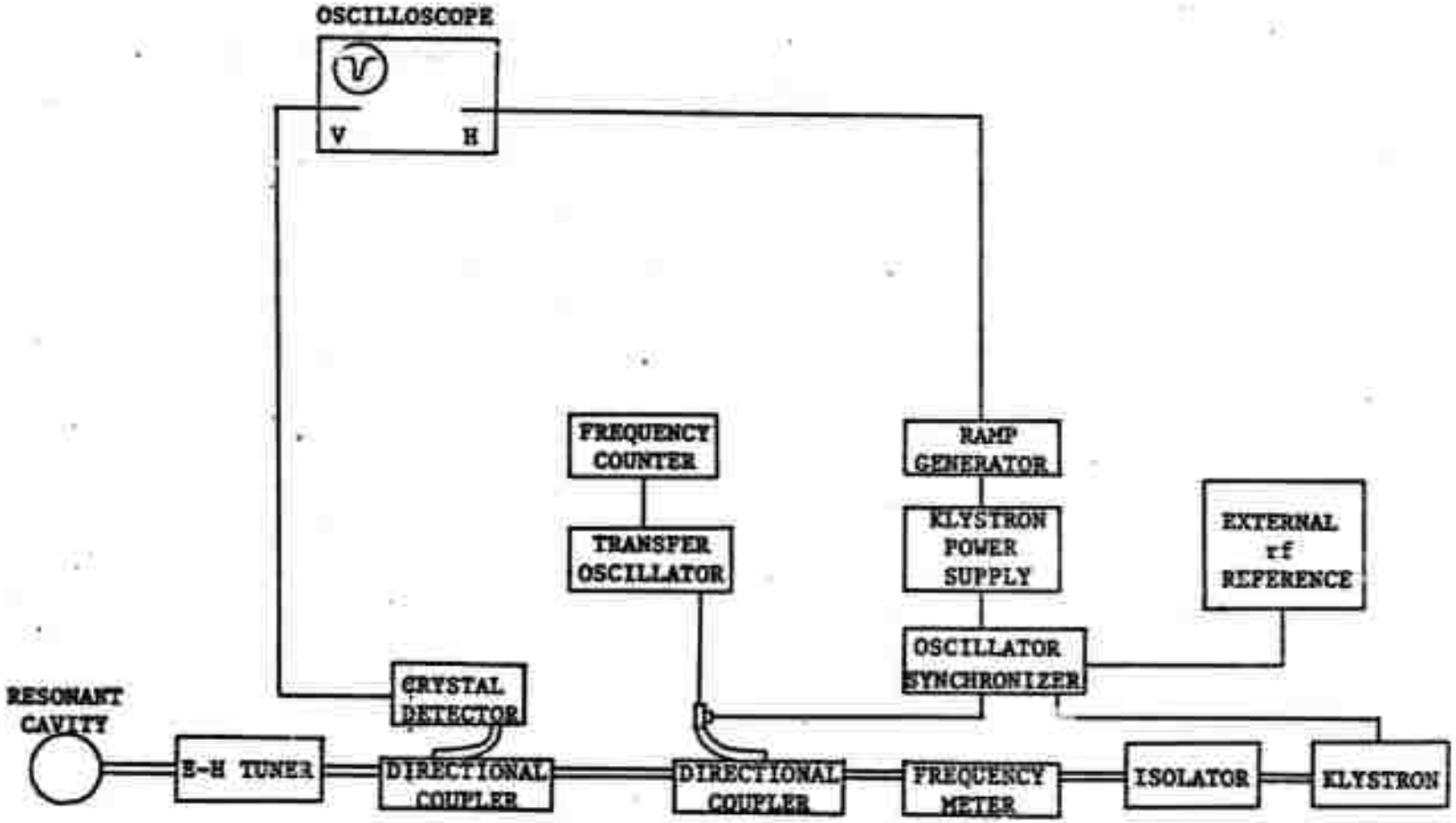

Fig. II-2 Microwave System

waveguide into the cavity is chosen to be magnetic for convenience. This is accomplished with an iris opening in the cylinder wall and a small wire loop mounted on a teflon holder. The plane of the loop is parallel with the short side of the waveguide. The wire can be moved in and out of the iris, thus varying the position of the loop in the TE-10 field pattern of the rectangular guide and the amount of coupling into the cavity. Figure II-3 shows the cavity-waveguide configuration with the sample in the position of maximum electric field and the loop for magnetic coupling.

The field equations for a cylindrical resonator in the TE-011 mode can be derived from Maxwell's equations

$$\nabla \times \bar{E} = - j\omega\mu\bar{H} \qquad (2.1)$$

$$\nabla \times \bar{H} = j\omega\epsilon\bar{E} \qquad (2.2)$$

and the wave equation in cylindrical coordinates for a TE wave propagating along the z-direction

$$\frac{\partial^2 H_z}{\partial r^2} + \frac{1}{r}\frac{\partial H_z}{\partial r} + \frac{1}{r^2}\frac{\partial^2 H_z}{\partial \phi 2} = -k_c^2 H_z \qquad (2.3)$$

where

H_z = the z-component of the magnetic field, H

$k_c^2 = \gamma^2 + \omega^2\mu\epsilon$

γ = propagation constant

by manipulating the above equation and applying the boundary condition that the tangential electric field must be zero the components of the electric and magnetic field expressions in cylindrical coordinates are obtained for the TE-011 cavity.

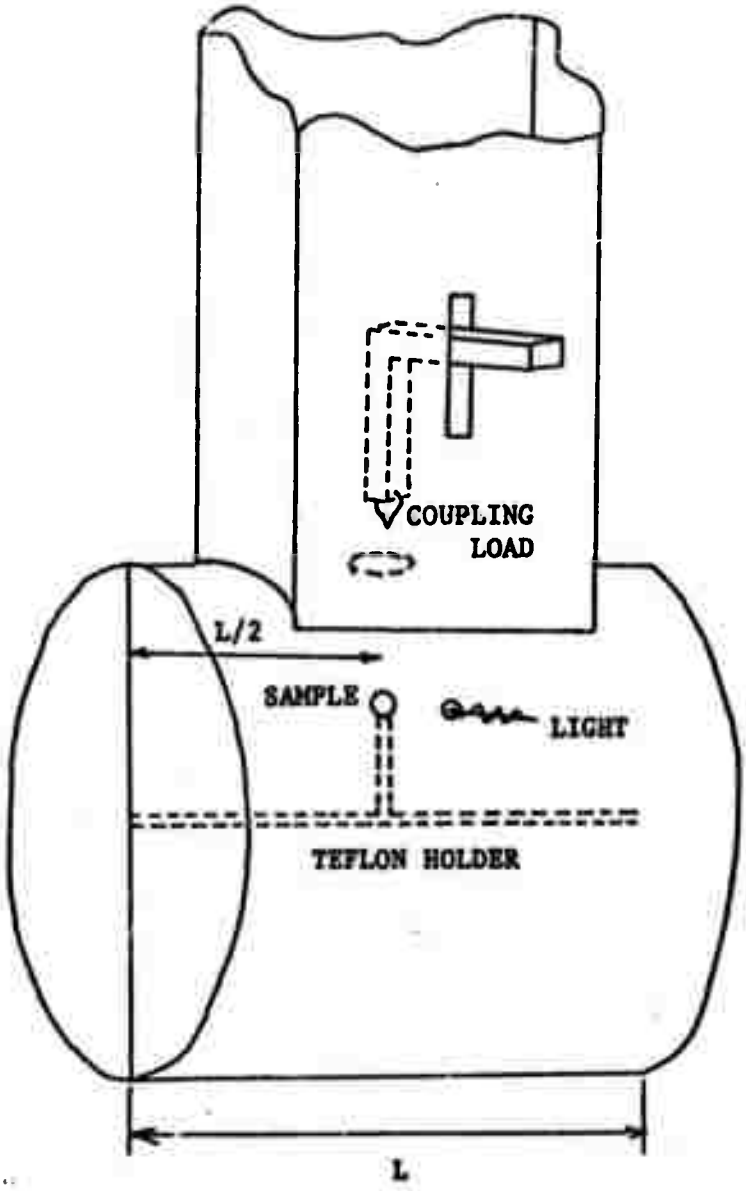

Fig. II-3 Cavity-Waveguide Configuration

$$H_z = -j2AJ_0(r\frac{P_{01}}{a})\sin\frac{\pi}{d}z \qquad (2.4)$$

$$E_\phi = 2A\eta\frac{f}{fc}J_0'(r\frac{P_{01}}{a})\sin\frac{\pi}{d}z \qquad (2.5)$$

$$H_r = -2A\frac{\eta}{Z_{TE}}\frac{f}{fc}J_0'(r\frac{P_{01}}{a})\cos\frac{\pi}{d}z \qquad (2.6)$$

$$H_\phi = E_r = E_z = 0 \qquad (2.7)$$

where

d = length of the cavity along z axis

$J_0(r\frac{P_{01}}{a})$ = a zero order bessel function

$Z_{TE} = \eta[1-(\frac{fc}{f})^2]^{-1/2}$

$\eta = \sqrt{\frac{\mu}{\epsilon}}$

A = a constant for the magnitude of the field

P_{01} = 3.81 (the first root $J_0'(x)=0$)

a = radius of the cavity

f_c = cutoff frequency

Klystron. A Varian X-13 reflex klystron with a frequency range of 8.1 to 12.4 GHz. is used as the microwave source. The klystron is powered by a Hewlett Packard Model 715A power supply.

Oscillator Synchronizer. The oscillator synchronizer is used to stabilize the klystron frequency which is prone to drift from its original setting. The instrument used is a Hewlett Packard Model DY-2650A which operates on the principle of automatic phase control (APC). A small sample (approximately -10dbm) of the

klystron's signal is mixed with a harmonic of the signal from a temperature stabilized crystal rf reference oscillator, either internal or external to the synchronizer, to produce a 30 Mlz i-f signal. This i-f signal is then phase compared to an i-f reference signal from a source, internal or external to the synchronizer. After the frequency is "locked", any attempts by the klystron to shift frequency produce a phase error and a phase comparator output error voltage. This voltage is applied in series with the klystron's repeller voltage to correct the frequency shift.

Transfer Oscillator. The Hewlett Packard Model 540B Transfer Oscillator is utilized to extend the range of the electronic counter into the x-band range of frequencies. The method used to determine frequency is to zero-beat the unknown input signal with a harmonic of an extremely stable signal generated internally and measure the fundamental of this internal signal on the counter.

2.5 Frequency Measurements

Measuring the exact resonant frequency of the TE-011 cavity required the use of the equipment discussed previously. In order to determine the frequency shift due to the change in the dielectric constant of the sample, the resonant frequency must be measured both before and after exciting the material.

The first step in frequency measurements is to obtain a mode pattern of the klystron on the oscilloscope. This is accomplished by modulating the klystron with a ramp signal and also using this

ramp to drive the horizontal sweep of the scope. The resulting pattern is shown in figure II-4. Next, the klystron is tuned to find the cavity resonance which is manifested as a small dip in the mode pattern since the cavity is operated in the reflection mode rather than transmission mode. This dip should be placed at the top of the mode pattern, as is shown in figure II-5, by tuning the klystron and the repeller voltage.

The klystron should then be placed in the cw mode and the ramp signal removed from the oscilloscope. This procedure will cause a single dot to appear on the scope. This is an unswept representation of the mode pattern and dip explained above. To tune the klystron to the exact resonant frequency of the cavity the repeller voltage should be adjusted to move the dot to the bottom of the dip.

Normally the frequency of the klystron is prone to drift from the desired setting so some type of stabilization is required. The klystron frequency is "locked" using the oscillator synchronizer discussed earlier. The APC switch on the synchronizer is turned to the on position and the klystron is locked by adjusting the external rf reference source (General Radio Oscillator, type 1208-B) until the search light goes out. The dot will now have to be returned to the bottom of the dip by adjusting the rf reference and VFO controls. Often it is not an easy matter to re-tune for resonance using the external rf reference and several attempts are usually necessary before the dot can be tuned to the desired point without loosing

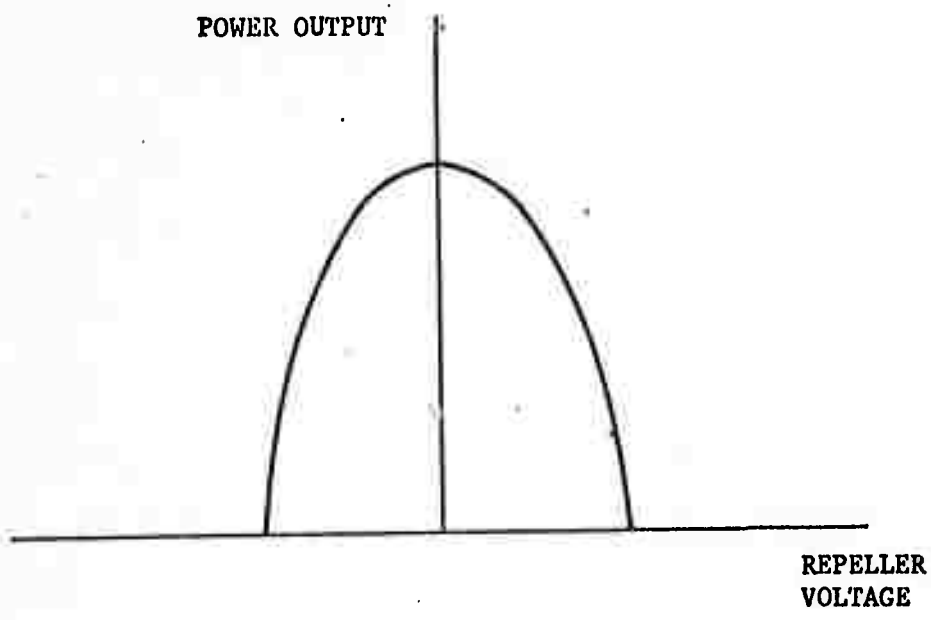

Fig. II-4 Klystron Mode Pattern

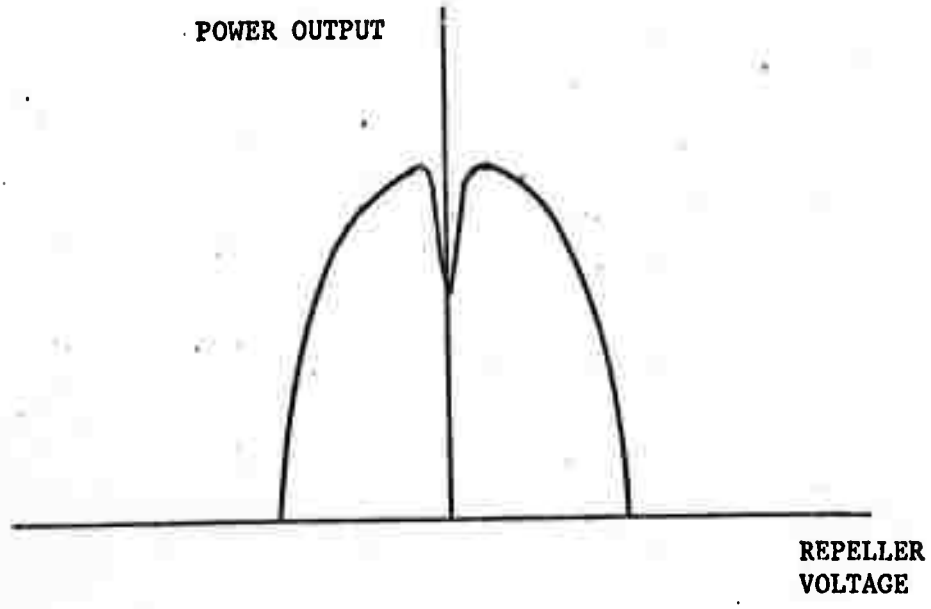

Fig. II-5 Resonant Frequency Dip

"lock".

The klystron is now tuned and locked to the exact resonant frequency of the cavity. This frequency is measured using the wavemeter, transfer oscillator and frequency counter. The frequency can be measured to two decimal places by tuning the wavemeter until its dip coincides with the cavity, causing the dot to drop further on the scope face. Then the transfer oscillator is tuned to a convenient fundamental frequency of that measured on the wavemeter. When this is reached a vertical deflection will be seen on the internal cathode ray tube. The gate control on the counter should now be set to the external reset position so that the counter will measure the transfer oscillator fundamental frequency at the precise moment that zero beat is reached. Now the fine vernier control should be tuned to reduce the difference-frequency to as close to zero as can be obtained. At the instant the zero beat is obtained, the counter reset button should be pressed to measure and record the frequency.

2.6 Optical Excitation

A He-Ne gas laser, LAS-2002, from Electro Optics Associates, was used to excite the amorphous sample. This laser produced a cw light with a wavelength of 6328 Å at a power of approximately 0.5 milliwatts. This wavelength corresponds to a photon energy of 1.965 eV. A projector lamp was also used as a white light source when a more powerful light source was needed.

In order to prevent unwanted light from exciting the sample prematurely, the dewar system was covered and a camera shutter was aligned with the lenses to provide precise control of the light.

2.7 Measurement of Cavity Q

In order to determine that the sample is effectively dominating the cavity, it is necessary to measure the Q of the empty cavity, and compare that to measurements of the Q of the cavity loaded with the teflon holder only and with the sample on the holder. A method developed by Ashley and Palka[14]) is used to make these Q measurements. The apparatus is assembled as shown in figure II-6 with the forward and reflected wave channels each connected to a vertical amplifier and the sweep output of the generator connected to the horizontal input. The oscilloscope is used in the chopped mode.

The sweep generator is adjusted to sweep through resonance and far enough on either side to present a complete view of the resonance dip. Slide screw tuner no. 1 is now adjusted so that no small dips or peaks appear in the incident wave. The vertical inputs to both channels are now grounded so that both levels can be adjusted to a common reference. Then the inputs are placed in the dc coupled mode and the two level-set attenuators just ahead of the detector mounts are set to equalize the detector outputs with the test resonator replaced by a good short.

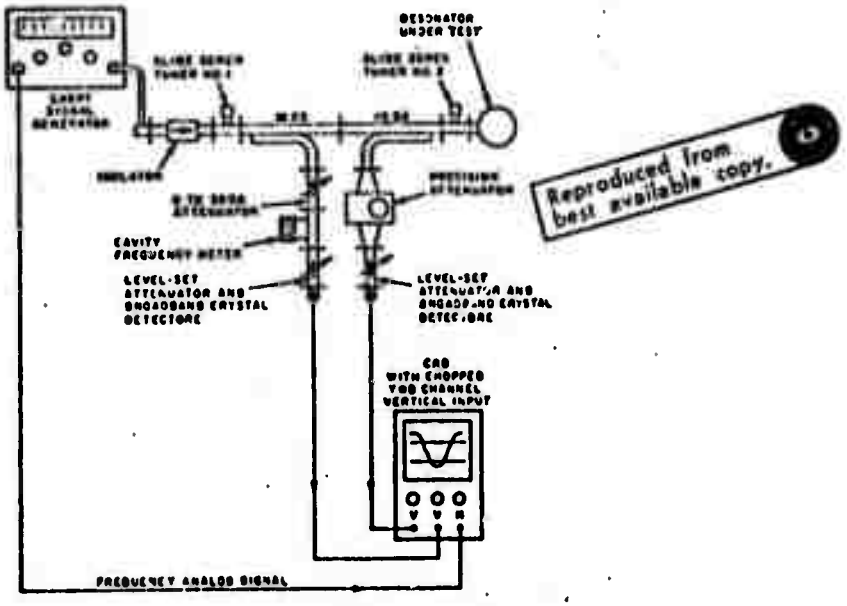

Fig. II-6 Apparatus for Q Measurement (ref. 14)

With the precision attenuator set to zero, the incident wave attenuator is adjusted to position the reference line at the bottom of the resonator dip. (Figure II-7a.) Now the precision attenuator is adjusted until the line from the resonant channel coincides with the line from the incident channel as shown in figure II-7b. The sweep generator may have to be tuned slightly off of resonance so that the flat top of the mode may be used in this alignment. The setting on the precision attenuator is a measurement of the reflection coefficient at resonance.

This value is now placed on the abscissa of figure II-8 (calculated by Ashley and Palka[14]) and another setting of the attenuator is read off the ordinate. The new setting will determine the half power bandwidth of the resonator. The precision attenuator is set to this new attenuation value and the forward wave channel attenuator is adjusted so that both reference lines coincide as shown in figure II-7c. Then all attenuation is removed from the reflected channel by returning the precision attenuator to zero dB. Figure II-7d shows the reflected channel dip, with all attenuation removed, and the forward wave channel crossing it. Now the bandwidth f_2-f_1 of the resonator is measured between the two crossings of the dip by the forward channel.

The oscilloscope screen grid is now calibrated in frequency so that the bandwidth can be read directly. This is accomplished by using the frequency meter to measure the total frequency change for

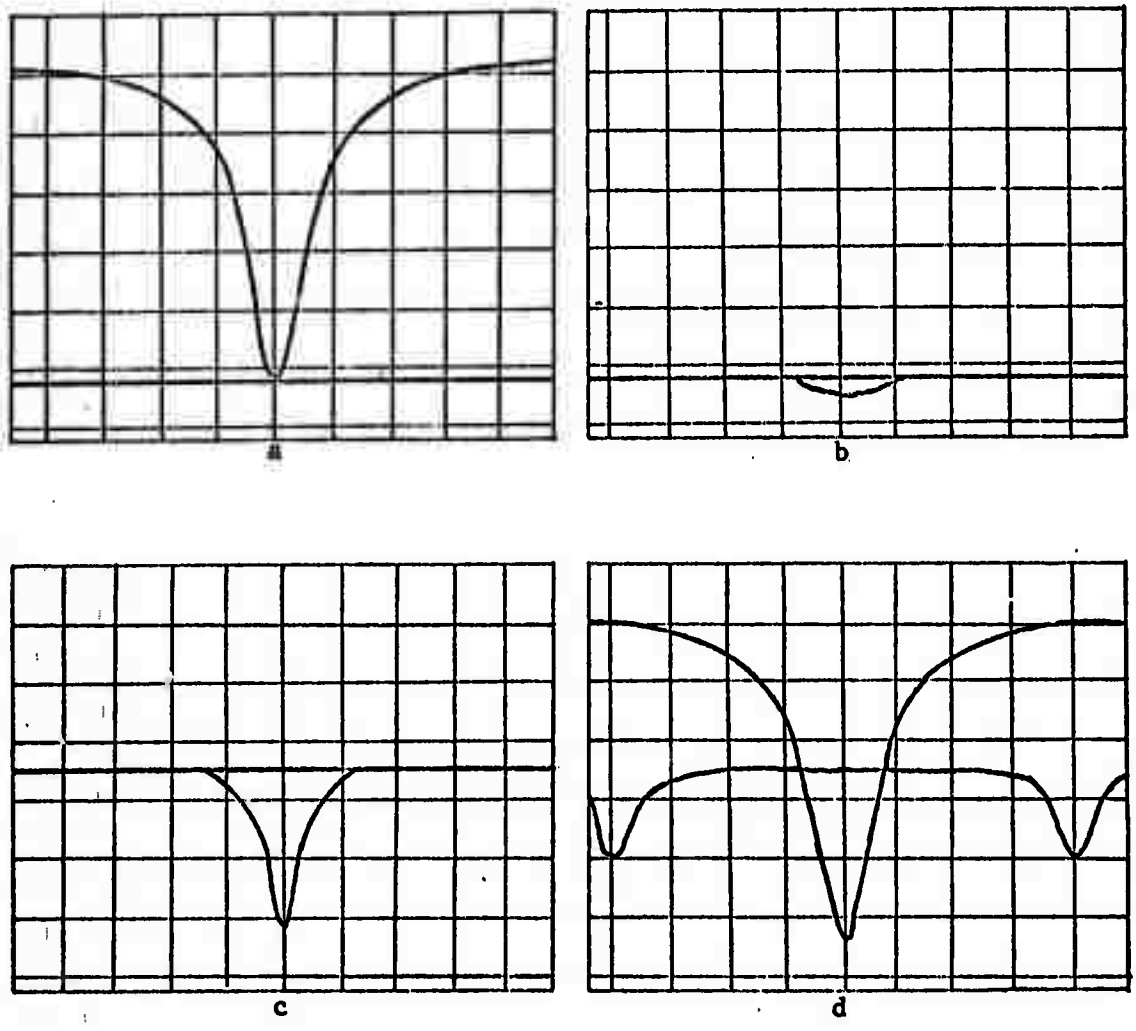

Fig. II-7 Oscilloscope Presentation of Q Data

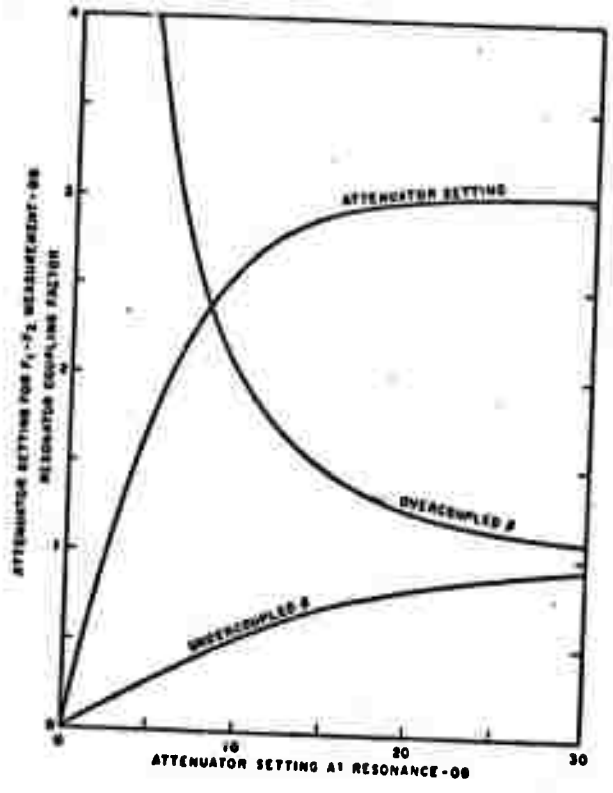

Fig. II-8 Beta and Attentuator Settings (ref. 14)

8 divisions along the horizontal (figure II-7d). If the analog voltage of the sweep generator is directly proportional to frequency over this limited range, then a simple measurement of length gives f_2-f_1.

Now the loaded Q is calculated as

$$Q_L = \frac{f_0}{f_2-f_1} \qquad (2.8)$$

where f_0 is the resonant frequency of the resonator.

To determine the unloaded Q of the cavity, Q_0, knowledge of the coupling factor β is required. However in this method of Q determination, it is sufficient to know only whether the cavity is overcoupled or undercoupled. Slide screw tuner no. 2, just ahead of the cavity, is used to determine this information. This tuner is adjusted until the reflection at resonance is small and then the tuner probe is withdrawn. If the bandwidth of the resonator decreases as the probe is removed, the cavity is undercoupled; but if the bandwidth increases, the cavity is overcoupled. When using this method to determine β, if the slide screw tuner is several wavelengths away from the cavity, care must be taken that the losses in the waveguide do not affect the measurements.

Using this information about coupling and the original precision attenuator setting, the value of β can be determined from figure II-8. This value of β is substituted into the following equation and the value of the unloaded Q is calculated.

$$Q_0 = (\beta + 1)\, Q_L \qquad (2.9)$$

CHAPTER III

RESULTS AND CONCLUSIONS

Several different samples of $2As_2Se_3 \cdot As_2Te_3$, As_2Se_3, As_2Te_3, As_2S_3 and Si(3%) Ge(4%) As(38%) Te(55%) were used in the photodielectric tests. These varied in size from about 0.3cm in diameter and 0.1cm thick to 0.75cm in diameter and 0.3cm thick. The G factors of these samples ranged from 0.00176 to 0.015. The experiment, as described in the previous chapter, was performed on these samples at room temperature, liquid nitrogen temperature (77°K) and liquid helium temperature (4.2°K), however, no photodielectric effect was observed.

In order to establish that the apparatus was not at fault, an Al doped sample of CdS, known to exhibit the photodielectric effect at 900 MHz, was tested. The equipment, described in Chapter II, performed properly and a frequency shift of 1.61 MHz was observed in the resonant frequency of 11.9 GHz, for full illumination from the HeNe laser. Q measurements were also conducted as described in the previous chapter, and it was determined that the sample dominated the loaded cavity. Thus any change in the sample polarization would be directly observable as a change in the resonant frequency, and any conductivity change would be reflected in the loaded Q of the cavity. In addition to establishing the integrity of the electronics, the alignment of the optics from the ambient, through

the liquified gases, into the cavity was verified.

In order to determine the general structure of the tested materials, X-ray diffraction methods were used. The results showed a generally disordered structure with some short range order existing. This data agrees with the existing theories which postulate the lack of long range order and the presence of some short range order in these types of materials.

Although only negative results were obtained for the five amorphous materials tested, it is premature to postulate the lack of a photodielectric effect to be a universal feature of disordered materials. However, it is appropriate to investigate known material properties of the amorphous chalcogenides to determine if some common denominator exists that would explain the apparent lack of depolarization. Therefore, this chapter discusses several possible explanations based upon the limited amount of data and partial theories that do exist.

3.1 Optical Absorption

Optical data on the material $2As_2Se_3 \cdot As_2Te_3$ is not available, but several authors give optical absorption and photoconductivity measurements for As_2Se_3, As_2Te_3, Te and Se. Rockstad[15]) measures an energy gap of 1.75eV in As_2Se_3 by optical methods and shows absorption data (figure III-1) for this and related materials. Davis and Shaw[16]) report data on amorphous As_2Se_3, Se and Te as

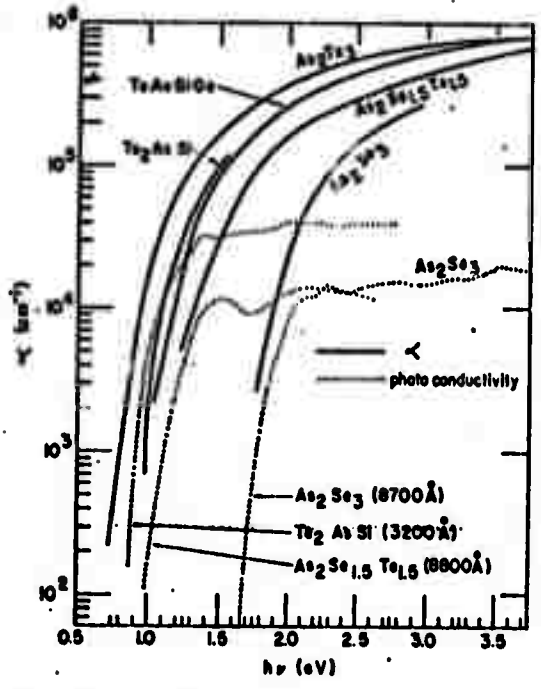

Fig. III-1 Optical Absorption Coefficient (ref. 15)

shown in figure III-2. These curves suggest that photon energy between 1.0 and 2.0eV might be used to excite the material under study. Edmond[17]) also reports optical absorption data on As_2Se_3 which supports these findings.

Optical absorption data is given by Fagen and Fritzsche[18]) on an amorphous material of the formula: Si(11%) Ge(11%) As(35%) P(3%) Te(40%) (type A material). Since this compound is predominately As and Te, the optical data should be applicable to the material under observation. Figure III-3 shows absorption data for the type A material which agrees with the reports of other authors on As_2Se_3. Figure III-4 also suggests the use of photons of energy greater than 1.0eV.

From the above optical absorption data, it is seen that the photon energy of the 6328 Å Laser light (~1.95eV) might have been marginal for band to band transitions in many of the materials. Therefore, a mercury arc lamp, containing lines from 3500 Å to 5461 Å, was used in duplicate tests. However these tests also failed to show any positive results.

Although sufficiently energetic photons were provided for band to band transitions or localized state to band transitions, there is uncertainty as to the number of created polarizable centers. In particular, if the available states in the forbidden band are considered, optical absorption data[19]) predicts an upper limit of $10^{16}eV^{-1}cm^{-3}$ gap states. However contradictory electrical data[19]) sets the density of gap states at $10^{19}eV^{-1}cm^{-3}$ in order to

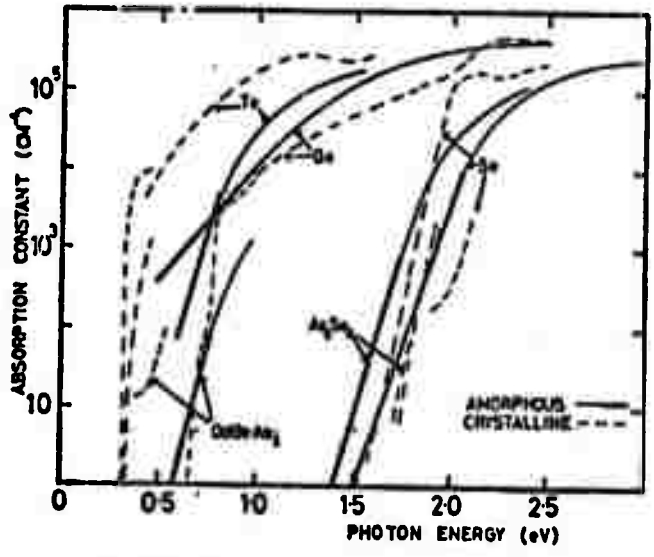

Fig. III-2 Optical Absorption Edges for As_2Se_3 (ref. 16)

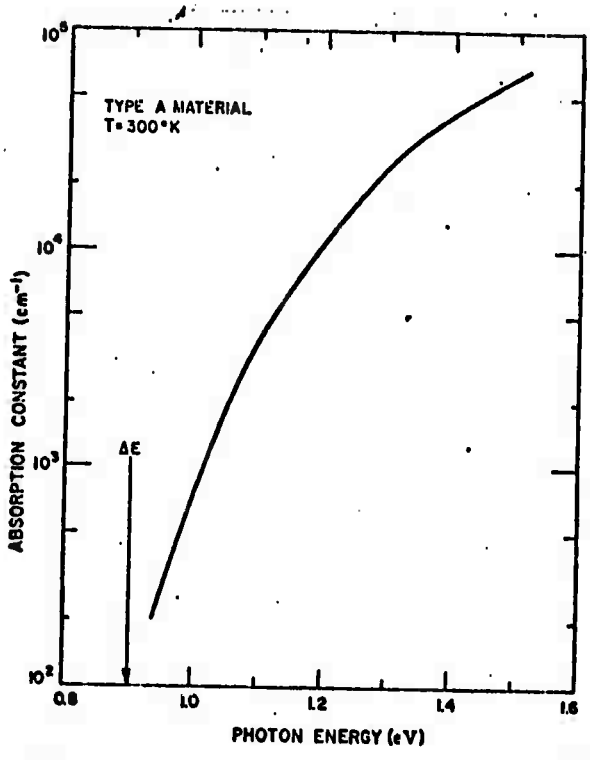

Fig. III-3 Absorption Constant for Type A Material (ref. 18)

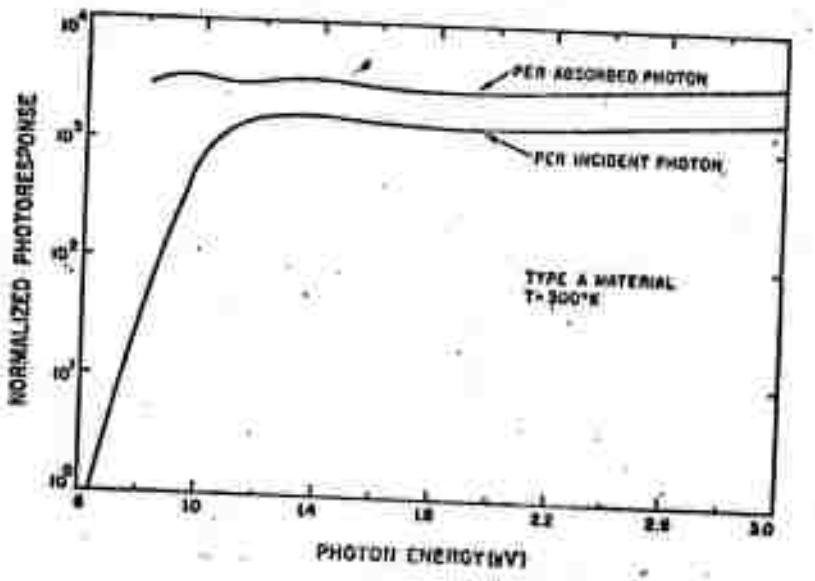

Fig. III-4 Photoresponse for Type A Material (ref. 18)

explain the lack of a field effect in several chalcogenides[19]). If the worst case condition is chosen, the density of states would be marginal for observation of polarization changes based on sensitivity predictions for the apparatus used by Hartwig and Hinds[2]). In addition, if the majority of the trapping sites are located deep in the forbidden band, Hartwig and Hinds show that the contributions to depolarization are small since the more tightly bound traps can provide smaller orbital changes and thus effect depolarization to a lesser extent.

Another possibility exists if the photon density is too low. If all created free carriers were used to fill the deep traps without ever saturating the less polarizable centers, then there would be no observable photodielectric effect nor would there be a Q change since there would be no conduction current to change the losses in the material. Because there is no charge injected in this electrodeless experiment, the contradictory observation of photoconductivity (with carrier injection) in the materials without a corresponding Q change when the material is in the cavity, is possibly explained. Before these suppositions can be proved or disproved, detailed thermally stimulated conductivity experiments will have to be performed to determine the trapping dynamics which are present.

3.2 Mobility Considerations

Benedict and Shockley[20]) describe the change in the real part of the dielectric constant by the equation

$$\varepsilon' = \varepsilon_\ell - \frac{ne^2}{\varepsilon_0 m^*} \frac{1}{[(e/m^*\mu)^2 + \omega^2]} \qquad (3.1)$$

where

ε_ℓ = the lattice dielectric constant

n = thermally generated carrier density

e/m^* = electron charge to effective mass ratio

ω = driving angular frequency

μ = mobility of free carriers

In analyzing the above equation it is evident that if the mobility of the free carriers is sufficiently low, then no dielectric change will be observed. Edmond[21]) suggests that in materials in the system As_2Se_3·As_2Te_3 there may be local fluctuations in the ratio of As_2Se_3 to As_2Te_3 causing a lowering of the effective mobility. Kolomiets and Lebedev[22]) and Hartke[23]) report that electron drift mobility in amorphous Se is lowered by the addition of a few atomic percent As or Te. Owen and Robertson[24]) show the low hole mobilities for As_2Se_3 for fields ranging from 9.4×10^4 to 55×10^4 V/cm (figure III-5).

3.3 Momentum Relaxation Time

Equations (1.19) and (1.31) show the importance of the carrier momentum relaxation time in determining the magnitude of the depolarization when the process is due to free carriers or trapping. Stone[3] has shown that the excitation frequency-relaxation time product must be greater than

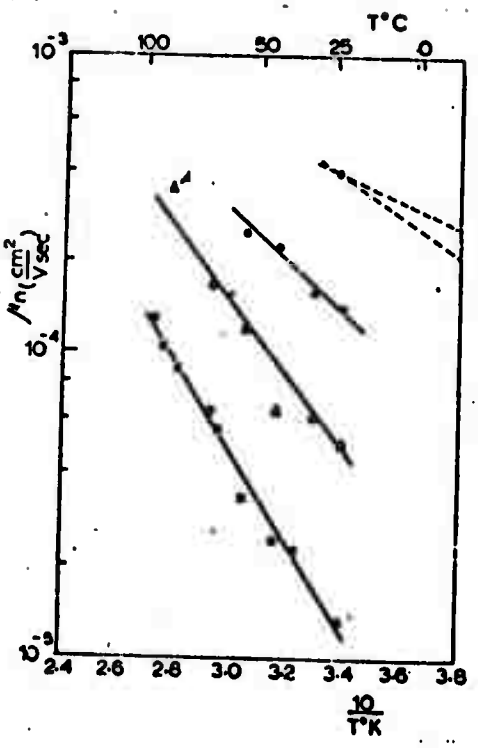

Fig. III-5 Drift Mobility for Holes in As_2Se_3 (ref. 23)

or approximately equal to unity for sufficient interactions of the created charge (free or bound) with the applied field. If $\omega\tau<<1$, then little or no photodielectric effect is observed. For an excitation of $\omega = 2\pi(11.8)10^9$, $\tau \leq 10^{-11}$ sec. would be sufficient to negate the photodielectric effect. Such a range of relaxation times in disordered materials is certainly possible since values of 10^{-12} sec. for intrinsic crystalline silicon at room temperatures are typical. Furthermore, the absence of an electron spin resonance signal (sensitivity of 10^{17} cm^{-3}) from chalcogenide films is attributed, by Fritzsche[19], to a short relaxation time, although no values are quoted.

The experiment at liquid helium temperature showed no photodielectric effect, thus, the upper bound on τ can be increased several orders of magnitude since τ should increase with decreasing temperature. It is interesting to consider the possibility of relaxation on the order of one lattice space which lead to relaxation times on the order of 10^{-15} sec.[18].

Figures 3.6, 3.7, and 3.8 show the effect of changing the momentum relaxation time for a cavity of resonant frequency 10^9 Hz. The effect at X-Band can be obtained by extrapolation since the effect of raising frequency is very nearly linear as far as the photodielectric response is concerned. The d/b ratio is simply a loading factor which will not be used other than to compare from one curve to the others. The overall effect is seen to be the decrease in photodielectric response (y-axis) as the relaxation time is decreased. The x-axis represents light power impinging on the sample.

3.4 Recommendations for Further Study

The energy levels of the trapping centers present in the energy gap can be determined more precisely by detailed thermally stimulated conductivity (TSC) experiments. In TSC measurements the electrical conductivity is obtained as a function of temperature. The procedure, outlined by Pickard and Davis[25]), employs photon excitation, at low temperatures, to generate free carriers which can be captured by trapping centers. After photon excitation the material is heated and the electrical conductivity is monitored as a function of the temperature. During the heating cycle, the bound carriers are freed from the traps, and the current measured in excess of the dark current is defined as the thermally stimulated current. Discrete trapping levels are indicated by the presence of peaks in the thermally stimulated current vs temperature curves. These peaks can be further analyzed to give information about the trap depth in energy, the capture cross section of the trap, and the density of trapping centers.

For future X-band frequency measurements, a plug in frequency extender for the electronic frequency counter should be obtained to replace the transfer oscillator. The method of zero-beat was found to be unreliable for measuring frequency changes of less than 0.1 MHz. Also, the practice of maintaining the exact resonant frequency while tuning for zero-beat was experimentally inaccurate because an exact zero-beat could only be approximated.

Additional optical equipment should be added to make the total apparatus adaptable to various different types of materials, both amorphous and crystalline. Also, a more sophisticated klystron power supply, providing internal ramp modulation, would simplify the experimental procedure and allow a whole mode pattern to be displayed on the oscilloscope at one time.

The existing microwave system, with these modifications, can be used as an effective tool to study the optical properties of many different semiconductor materials.

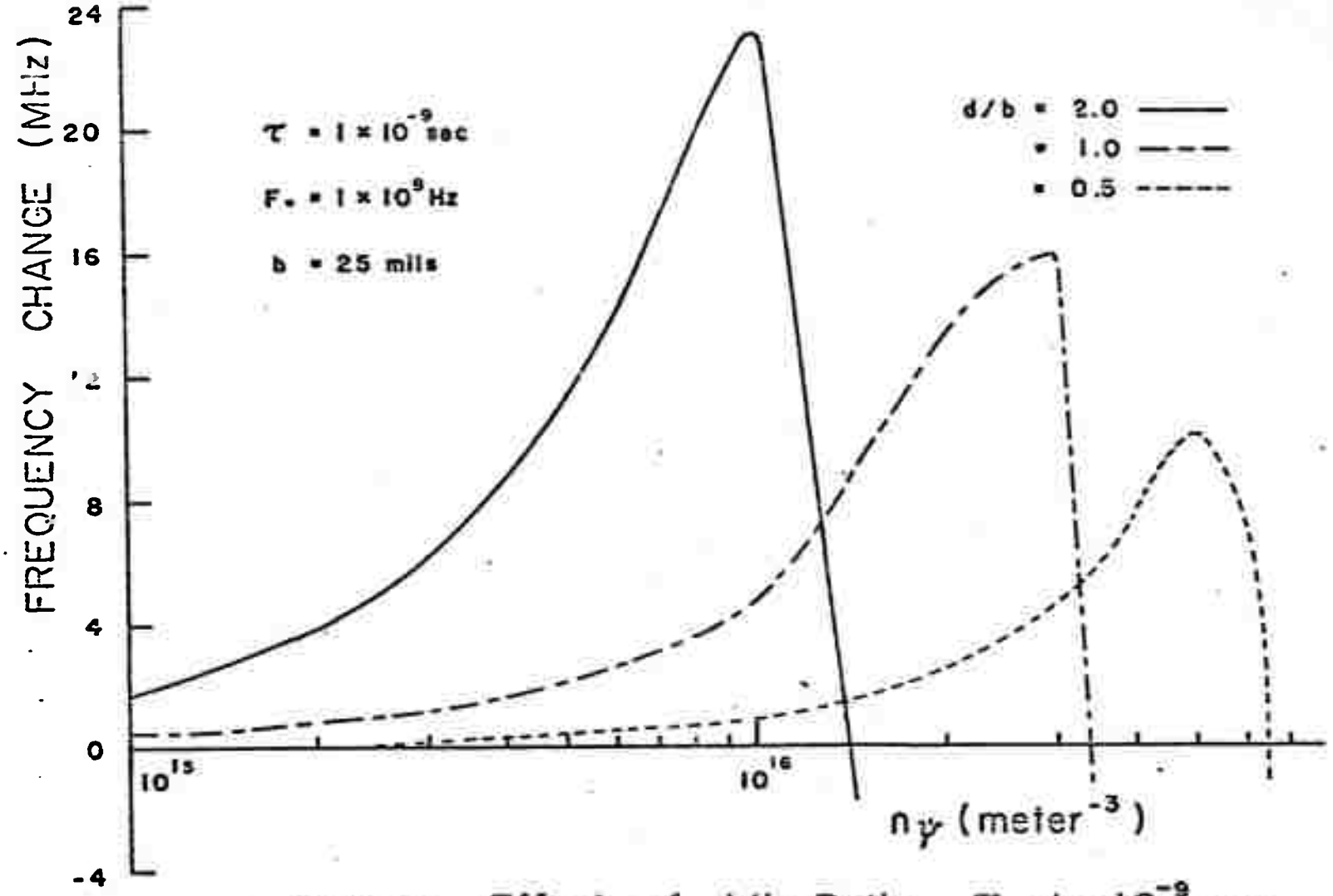

Figure 3.6 Effect of d/b Ratio, $\tau = 1 \times 10^{-9}$ sec

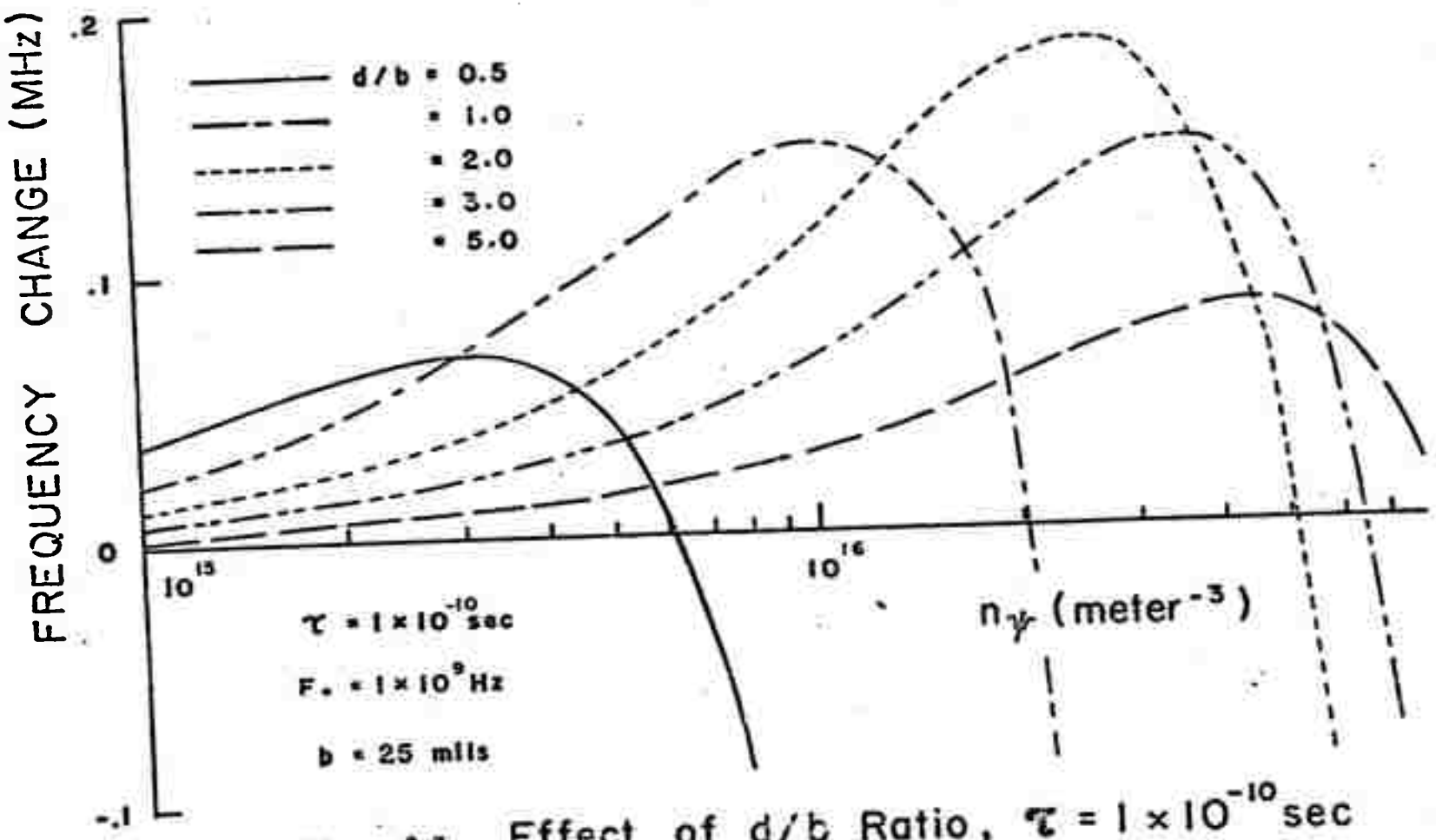

Figure 3.7 Effect of d/b Ratio, $\tau = 1 \times 10^{-10}$ sec

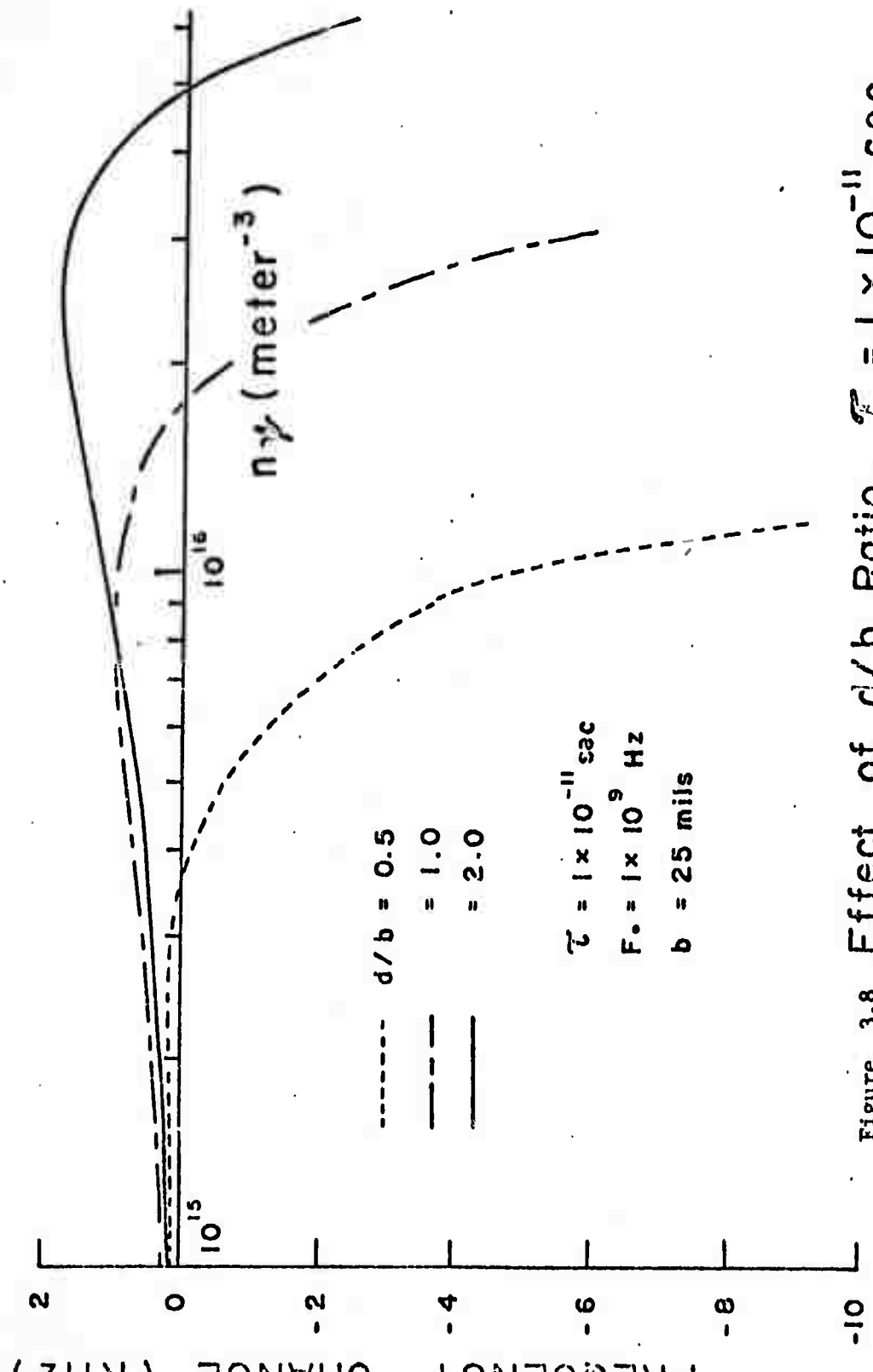

Figure 3.8 Effect of d/b Ratio, τ = 1 x 10^{-11} sec

REFERENCES

1) G. D. Arndt, W. H. Hartwig and J. L. Stone, J. Appl. Phys. 39 (1968) 2653.

2) W. H. Hartwig and J. J. Hinds, J. Appl. Phys. 40 (1969) 2020.

3) J. L. Stone, Ph.D. Dissertation, University of Texas (1968).

4) M. Sucher and J. Fox, Handbook of Microwave Measurements (Interscience Publishers, New York, 1963).

5) G. D. Arndt, Ph.D. Dissertation, University of Texas (1966).

6) R. H. Bube, Photoconductivity of Solids (Wiley, New York, 1960).

7) J. J. Hinds, Master's Thesis, University of Texas (1968).

8) M. H. Cohen, J. Non-Crystalline Solids 2 (1970) 432.

9) M. H. Cohen, H. Fritzsche, S. R. Ovshinsky, Phys. Rev. Letters 22 (1969) 1065.

10) A. M. Andriesh and B. J. Kolomiets, Soviet Phys.-Solid State 5 (1963) 1063.

11) J. Botila and A. Vancu, Mater. Res. Bull. 5 (1970) 925.

12) B. J. Kolomiets, V. M. Lyubin and V. L. Averjanov, Mater. Res. Bull. 5 (1970) 655.

13) E. A. Fagen and H. Fritzsche, J. Non-Crystalline Solids 2 (1970) 180.

14) J. R. Ashley and F. M. Palka, The Microwave Journal 14 (1971) 35.

15) H. K. Rockstad, J. Non-Crystalline Solids 2 (1970) 192.

16) E. A. Davis and R. F. Shaw, J. Non-Crystalline Solids 2 (1970) 406.

17) J. T. Edmond, Brit. J. Appl. Phys. 17 (1966) 979.

18) E. A. Fagen and H. Fritzsche, J. Non-Crystalline Solids 4 (1970) 480.

19) H. Fritzsche, J. Non-Crystalline Solids 6 (1971) 49.

20) T. S. Benedict and W. Shockley, Phys. Rev. 91 (1953) 1565.

21) J. T. Edmond, J. Non-Crystalline Solids 1 (1968) 39.

22) B. T. Kolomiets and E. A. Lebedev, Soviet Phys.- Solid State 8 (1966) 905.

23) J. L. Hartke, Phys. Rev. 125 (1962) 1177.

24) A. E. Owen and J. M. Robertson, J. Non-Crystalline Solids 2 (1970) 40.

25) P. S. Pickard and M. V. Davis, J. Appl. Phys. 41 (1970) 2636.

APPENDIX I

AMORPHOUS MATERIAL PROCESSING

The procedure used in making the amorphous material is begun by sealing off one end of a vycor tube, using an oxy-hydrogen torch. To light the torch, the hydrogen regulator is set to 5 lbs. pressure and the oxygen regulator is set to 15 lbs. The oxygen is turned on to purge the line and then turned off completely. The hydrogen line is opened until a small flow can be felt at the nozzle. This small stream is then lit and the oxygen is turned on and adjusted until the desired flame is produced.

After one end of the tube has been sealed by twisting it while soft, the vycor is then cleaned. In this procedure, nitric acid is used as the cleaning agent and is followed by DI water and alcohol rinses.

The correct amount of each of the constituents is weighed on an analytical balance and then loaded into the cleaned vycor tube. This is then evacuated using a vacuum pump and sealed with the torch. When sealing the vycor, the tube is heated evenly in an area near the open end and the vacuum is allowed to suck in the sides slightly. After the glass is softened, it is twisted and pulled apart at this indentation, thus sealing the material in an evacuated ampoule.

The torch is then extinguished by first turning off the oxygen

and then the hydrogen. When all the hydrogen is exhausted, a distinctive pop is heard. Then both main valves should be turned off and both lines bled off.

The sealed ampoule is then placed in the quartz boat and inserted into the oven (preheated to 800°C) and allowed to remain for 8 hours. During the last hour in the oven, the sample is agitated by rocking to assure a uniform mixture of all components. At the end of the 8 hour period the ampoule is removed and quinched either slowly at room temperature or quickly in a water bath. The sample is then extracted by breaking the glass capsule.

APPENDIX II

OVEN CONTROL CIRCUIT

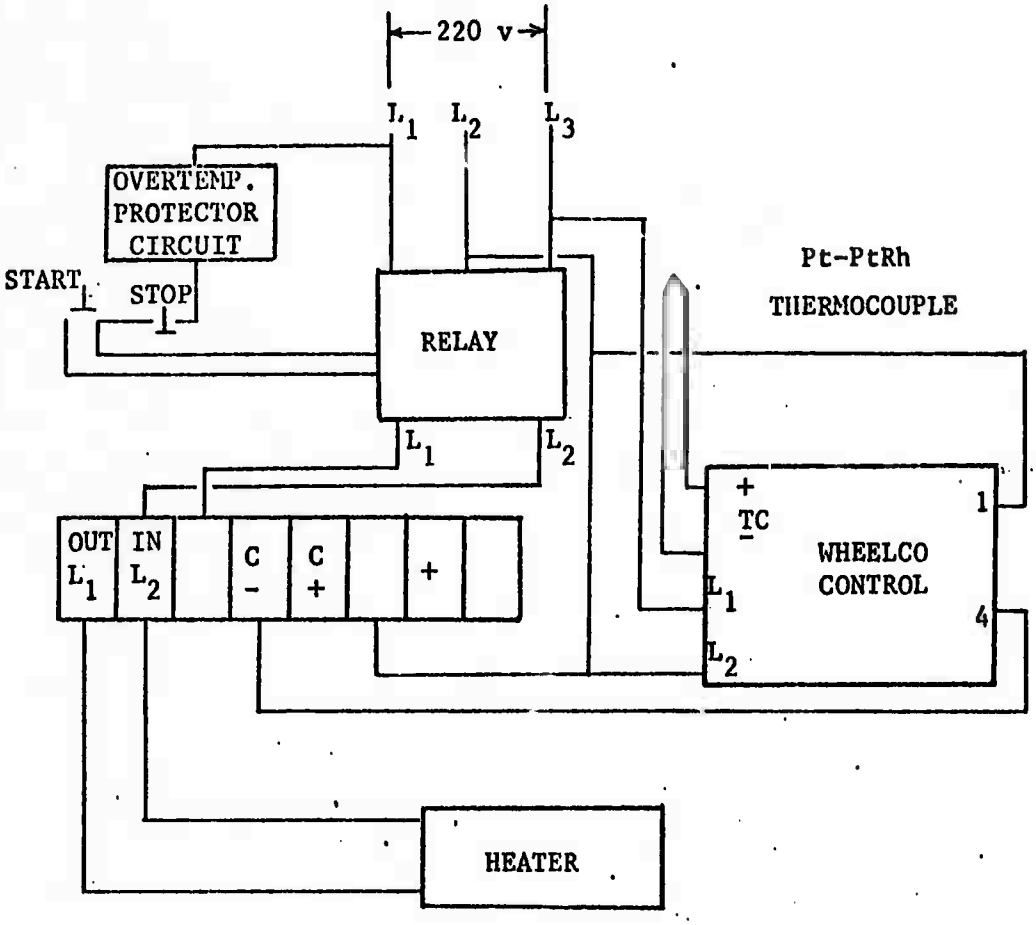

Note: If the overtemperature protective circuit shuts off the system, the switch must be rotated to off and then back to the limit position in order to engage the relay.

PART II

CHAPTER I

THE THERMALLY STIMULATED CONDUCTIVITY

Introduction

In recent years considerable attention has been focused on amorphous or non-crystalline materials. Although many of the features of these materials strongly resemble those of more conventional and better understood crystalline materials, several important properties are found to deviate radically[1-3]. In an attempt to explain the behavior of these materials, several theories and models have been proposed[4-13]. Cohen, Fritzsche, and Ovshinsky[7-12] have done extensive research on various amorphous materials and have proposed a model (commonly called the CFO model) which departs radically from the theory of single crystal materials. The most important differences of the CFO model include the absence of an energy band gap in the density of states (see Figure I-1), and the existence of a mobility gap in which the carrier mobility is extremely small. Moreover, the states in the "mobility gap" are spacially localized (since the mobility is very small), and the density of these localized states is approximately equal to the effective density of states at the "conduction" band edge[12].

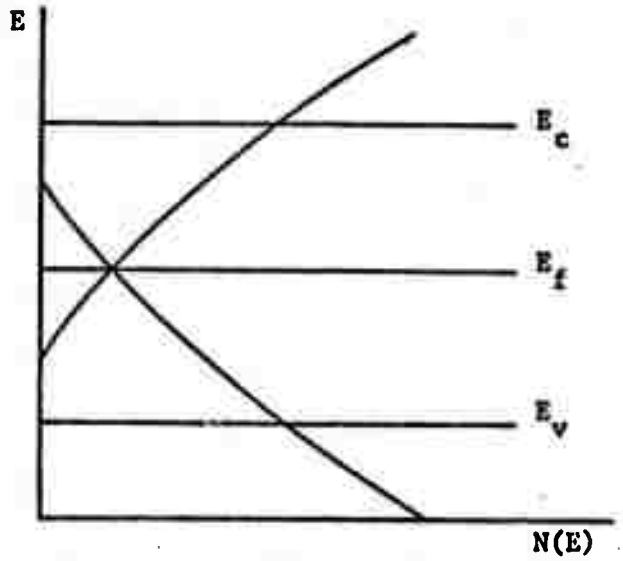

(A)

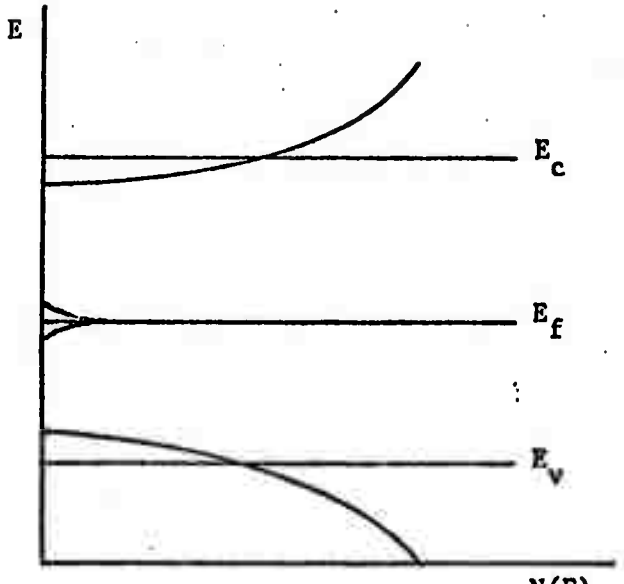

(B)

Figure I-1 Proposed Density of States as Function of Energy for (A) CFO model and (B) Mott-Davis model (ref. 13)

Mott and Davis[13] have proposed a theory based on the extension of the theory of the degenerate semiconductor. The Mott-Davis model includes an energy band gap with a narrow (< 0.1 eV) band of localized states existing in the bandgap at the Fermi level as shown in Figure I-1 (page 58).

Among the many amorphous materials which have been studied, some of the more common are in the family of the so called chalcogenide glasses which include the various compounds of S, Se, and Te. The purpose of this thesis is to report on research done on a particular binary compound of this family, As_2Se_3. Kolomiets and Lebedev[14] have investigated thin film amorphous As_2Se_3 by the method of space charge limited currents and report a continuous density of localized states near the Fermi level with a density of $3 \times 10^{15} - 1.5 \times 10^{16}$ cm^{-3} eV^{-1}. Kolomeits and Mazets[15] have performed th thermally stimulated conductivity experiment qualitatively on amorphous As_2Se_3 in the bulk and conclude a continuous distribution of localized states in the energy range of .35 to .75 eV. The thermally stimulated conductivity (TSC) experiment was chosen for this research so that the density of localized states in the "band gap" could be investigated. From the results of this experiment, it is possible to determine how the various models apply to this material.

Theory

The Mott-Davis model postulates a quasi-discrete density of localized states or trapping levels at the Fermi level in amorphous materials. The CFO model postulates that a quasi-continuous density of localized states or trapping levels exists. In order to test these hypotheses, the TSC experiment was chosen to investigate the trapping levels in the material under study. In order to simplify the explanation of the theory of the TSC experiment, two discussions are given; a qualitative description of the experiment itself, and a discussion of the equations applicable to the experiment.

Qualitative Description

It is assumed in the following discussion that the experiment is done on a semi-insulating crystal with one trapping level (at E_t) in the band gap as shown in Figure I-2A, and that retrapping does not occur.

At room temperature a finite number of carriers will be present in the conduction band. If the crystal is cooled, part of these carriers will lose thermal energy and fall down into the valence band. At very low temperatures (below liquid nitrogen temperature) essentially all of the carriers will be in the valence band.

If energy is pumped into the crystal while maintaining the

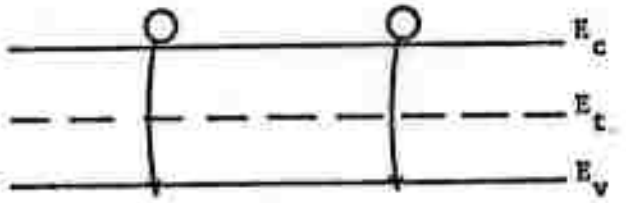

(A)

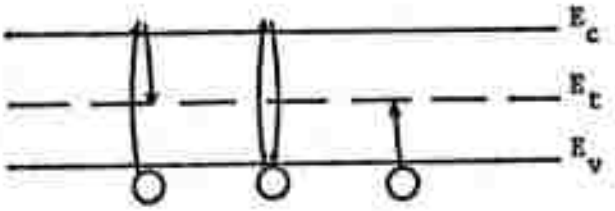

(B)

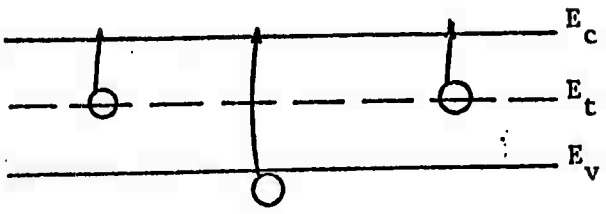

(C)

Figure I-2 Band Diagram of a Crystal with One Trapping Level at E_t

low temperature (for example, by a light source) carriers will be excited out of the valence band to the conduction band or to a trap. However, those which reach the conduction band do not have enough thermal energy to remain there and fall back to a trap or the valence band as shown in Figure I-2B (page 61). If this process is continued long enough, the traps will eventually become saturated.

If the crystal is then heated at some rate, the electrons in the traps will begin to gain thermal energy and will be excited to the conduction band as shown in Figure I-2C (page 61). These electrons will cause the conductivity of the material to increase. As the traps empty, this increase in conductivity will reach a maximum and begin to decrease back to the dark value. By analyzing the change in conductivity, information can be obtained about the traps such as their energy depth and their density.

If the material has more than one trapping level, the TSC plot will have a corresponding number of peaks which may be analyzed independently. However, if the material is characterized by the CFO model, the trapping sites are quasi-continuous, and hence, no discrete peaks should be observed.

Quantitative Analysis

The TSC experiment has been conducted by various investigators, and several forms of analysis for the TSC curves exist[16-25]. However, none of the above authors consider the general case with

both retrapping and recombination effects. Dussel and Bube[26] have considered the problem in a general way, but their results are much too complicated to be of practical value. Haine and Carley-Read[27] have derived simpler expressions describing the form of the TSC curve irrespective of whether or not retrapping occurs. A summary of the derivation presented by Haine and Carley-Read is given below.

Analysis for discrete trapping levels. Three rate processes are important in analyzing TSC curves. These are the rate of release of electrons from trapping levels, the rate of retrapping of electrons, and the rate of recombination. These rates can be combined into a general equation:

$$\frac{dn_c}{dt} = \frac{n_t \Theta}{T_t} - \frac{n_c}{T_t}\left(1 - \frac{n_t}{N_t}\right) - \frac{n_c}{T} \qquad \text{(I-1)}$$

where: n_c is the density of electrons in the conduction band

n_t is the density of electrons in the trapping level

N_t is the equivalent density of trapping centers

Θ is the trapping factor [$\Theta = N_c/N_t \exp(-E_t/kT)$]

N_c is the equivalent density of states in the conduction band

E_t is the depth of the trapping level

k is Boltzman's constant

T is the temperature in degrees Kelvin

T_t is the trapping time

T is the recombination lifetime

t is time.

If the experiment is performed at a slow rate, any change in n_c with respect to time can be neglected ($dn_c/dt = 0$), and Equation (I-1) can be solved for n_c. By differentiating with respect to temperature and neglecting the temperature dependence of N_c, an equation for the trap density described by the slope at any point on the TSC curve can be derived and is given as:

$$N_t(T + T_t) = \frac{\{N_c + N_c \exp(-E_t/kT)\}^2}{\frac{dT}{dt} N_c\{E_t/kT^2 - \frac{dn_c}{dT}/n_c\}\exp(-E_t/kT)} \qquad \text{(I-2)}$$

At a current maximum, $dn_c/dT = 0$, and Equation (I-2) can be simplified to:

$$N_t(T+T_t) = \frac{kT^2 N_c}{E_t \frac{dT}{dt}} \exp(-\frac{E_t}{kT})\{1+ \frac{n_c}{N_c} \exp(\frac{E_t}{kT})\}^2 \qquad \text{(I-3)}$$

Equation (I-3) has N_t in terms of E_t, the trapping level. Bube[28] gives the trapping level as:

$$E_t = kT_m \, \text{LOG}(\frac{N_c}{n_{cm}}) \qquad \text{(I-4)}$$

where: n_{cm} is the density of electrons in the conduction band at a current maximum, T_m is the temperature at the maximum, and the logarithm is to the base e.

Therefore, by use of Equation (I-3) and Equation (I-4), E_t and N_t can be found from the TSC maximum.

Analysis for quasi-continuous trapping levels. The previous

analysis assumes that the material has discrete trapping levels. In the case of quasi-continuous trapping levels (as postulated by the CFO model), the analysis must be extended. In the following discussion, it is assumed that electrons move from traps only to the conduction band, and that thermal equilibrium is effectively maintained between the trapping levels and the conduction band. That is, for a given temperature, the Fermi level lies at the energy level E, and all the trapping levels above this level are effectively empty whereas the trapping levels below E are effectively full. As the temperature is increased, trapping levels further down in energy empty, and the Fermi level moves toward the valence band a corresponding amount. Therefore, Equation (I-4) is still applicable. It is also assumed that any retrapping which occurs is effectively at the level E since carriers which are retrapped at levels above E have enough thermal energy to return to the conduction band, and the states below E are full so retrapping cannot occur. There are three important processes for the analysis.

(1) Rate of release of electrons from traps (R_R)

$$R_R = \frac{n_t \Theta}{T_t} \qquad \Theta = \frac{N_c}{N_t} \exp\ (-E/kT) \qquad \text{(I-5)}$$

where: T_t is the trapping time for an electron by trapping level with zero occupancy.

$n_t = n_t(E)$ is the density of electrons at trap level E.

N_c is the equivalent density of states at the bottom of the conduction band.

$N_t = N_t(E)$ is the density of traps at E.

E is the energy depth below E_c.

k is Boltzman's constant.

T is the absolute temperature.

(2) Rate of retrapping of electrons (R_T)

$$R_T = \frac{n_c[1-f(E)]}{T_t} \qquad \text{(I-6)}$$

where: $n_c = n_c(E)$ is the density of electrons in the conduction band.

f(E) is the Fermi function.

(3) Rate of Recombination (R_C)

$$R_C = \frac{n_c}{T} \qquad \text{(I-7)}$$

where: T is the recombination lifetime.

These processes are related by:

$$\frac{dn_c}{dt} = R_R - R_T - R_C = \frac{n_t\Theta}{T_t} - \frac{n_c}{T_t}[1-f(E)] - \frac{n_c}{T} \qquad \text{(I-8)}$$

It is now assumed that dn_c/dt can be neglected since the experimental rate of change of n_c is very small compared to the relaxation time of n_c (smaller of T or T_t) after a perturbation in the flow processes[27].

$$\rightarrow \quad \frac{n_t\Theta}{T_t} = \frac{n_c}{T_t}[1-f(E)] + \frac{n_c}{T}$$

or

$$n_c = \frac{n_t\Theta}{1 + T_t/T - f(E)} \qquad \text{(I-9)}$$

Taking derivitives with respect to E:

$$\frac{dn_c}{dE} = \frac{\Theta \frac{dn_t}{dE} + n_t \frac{d\Theta}{dE}}{1 + T_t/T - f(E)} + \frac{n_t \Theta \frac{df(E)}{dE}}{\{1 + T_t/T - f(E)\}^2} \qquad \text{(I-10)}$$

(Assuming that T_t and T are constant. The assumption for T_t is justified if N_t does not vary widely since T_t is inversely proportional to N_t. This assumption is valid for the CFO model since N_t is postulated to be approximately equal to N_c).

But,

$$\Theta = \frac{N_c}{N_t} \exp(-E/kT) \rightarrow \frac{d\Theta}{dE} = -\frac{\Theta}{kT} - \frac{\Theta}{N_t}\frac{dN_t}{dE} \qquad \text{(I-11)}$$

(the temperature dependence of N_c is neglected)

and,

$$f(E) = \frac{dn_t}{dN_t} = \left[1 + \exp\left\{\frac{E-Ef}{kT}\right\}\right]^{-1} \qquad \text{(I-12)}$$

$$\rightarrow \quad \frac{df(E)}{dE} = \frac{f^2(E)}{kT} \exp\left(\frac{E-Ef}{kT}\right) \qquad \text{(I-13)}$$

Define:

$$g(E) = \frac{dN_t}{dE} \qquad \text{(I-14)}$$

Substituting (I-11), (I-12), (I-13), and (I-14) into (I-10) gives:

$$\frac{dn_c}{dE} = \frac{\Theta\left[f(E)g(E) - \frac{n_t}{kT} - \frac{n_t g(E)}{N_t}\right]}{1 + T_t/T - f(E)} - \frac{n + \Theta f^2(E) \exp(E-Ef)/kT}{\{1+T_t/T-f(E)\}^2} \qquad \text{(I-15)}$$

Equation (I-9) gives:

$$n_t = \frac{n_c[1+T_t/T-f(E)]}{\Theta} \qquad \text{(I-16)}$$

Substituting (I-16), combining, and simplifying gives:

$$\frac{dn_c}{dE} = g(E)\left[\frac{\Theta f(E)}{1+T_t/T-f(E)} - \frac{n_c}{N_t}\right] - \frac{n_c}{kT}\frac{f^2(E)\exp\left(\frac{E-Ef}{kT}\right)}{\{1+T_t/T-f(E)\}} + \frac{n_c}{kT} \qquad \text{(I-17)}$$

From Equation (I-5),

$$\Theta = \frac{N_c}{N_T}\exp\left(\frac{-E}{kT}\right)$$

$$+ g(E)\left[\frac{N_c\exp\left(\frac{-E}{kT}\right)f(E)}{1+T_t/T-f(E)} - n_c\right] - N_t\left[\frac{n_c f^2(E)\exp\left(\frac{E-Ef}{kT}\right)}{kT\{1+T_t/T-f(E)\}} - \frac{n_c}{kT} + \frac{dn_c}{dE}\right] = 0 \qquad \text{(I-18)}$$

Let:

$$A(E) = \frac{N_c\exp\left(-\frac{E}{kT}\right)f(E)}{1+T_t/T-f(E)} - n_c \qquad \text{(I-19)}$$

and

$$B(E) = \frac{n_c f^2(E)\exp\left(\frac{E-Ef}{kT}\right)}{kT\{1+T_t/T-f(E)\}} - \frac{n_c}{kT} + \frac{dn_c}{dE} \qquad \text{(I-20)}$$

And:

$$g(E) = \frac{dN_t}{dE} \qquad \text{(I-14)}$$

Thus:

$$A(E)\frac{dN_t}{dE} - B(E)N_t = 0$$

or

$$\frac{dN_t}{dE} - \frac{B(E)}{A(E)}N_t = 0 \qquad \text{(I-21)}$$

But, Equation (I-4) defines the relationship between E and T:

$$E = kT\,\mathrm{Log}_e\left(\frac{N_c}{n_c}\right) = CT \qquad \text{(I-4)}$$

Making the above change of variables in Equation (I-21) gives:

$$\frac{dN_t}{dT} - \frac{\frac{dE}{dT}\,B(CT)}{A(CT)}\,N_t = 0 \qquad \text{(I-22)}$$

Let:

$$H(T) = \frac{\frac{dE}{dT}\,B(CT)}{A(CT)} \qquad \text{(I-23)}$$

$$\rightarrow \quad \frac{dN_T}{dT} - H(T)\,N_T = 0 \qquad \text{(I-24)}$$

$$\rightarrow \quad N_T = N_c \exp\left[\int_0^T H(T)\,dT\right] \qquad \text{(I-25)}$$

Equation (I-25) lends itself to a simple computer solution provided the various material parameters are known.

CHAPTER II

EXPERIMENTAL APPARATUS AND TECHNIQUES

Experimental Apparatus

A block diagram of the system designed and built to perform the TSC experiment is shown in Figure II-1. Three main divisions of the apparatus require special attention namely the sample holder, the sample heater, and the data recorder.

Sample Holder

The design of the sample holder was determined by the choice of the sample geometry. Several alternatives were considered, and the structure shown in Figure II-2 was chosen. Thin film aluminum side-by-side contacts are deposited on a glass substrate, and the amorphous material is then deposited in the space separating the contacts. The spacing can be varied and carefully controlled for repeatability by using standard photolithographic techniques. The holder design was completed as shown in Figure II-3 subject to the physical restraints of the Dewar system and the apparatus necessary to perform the experiment.

A chromel-constantan thermocouple with a liquid nitrogen reference was chosen to monitor the temperature due to its relatively high output voltage over the temperature range of interest (see Figure II-4). The heater is composed of four, forty-seven ohm,

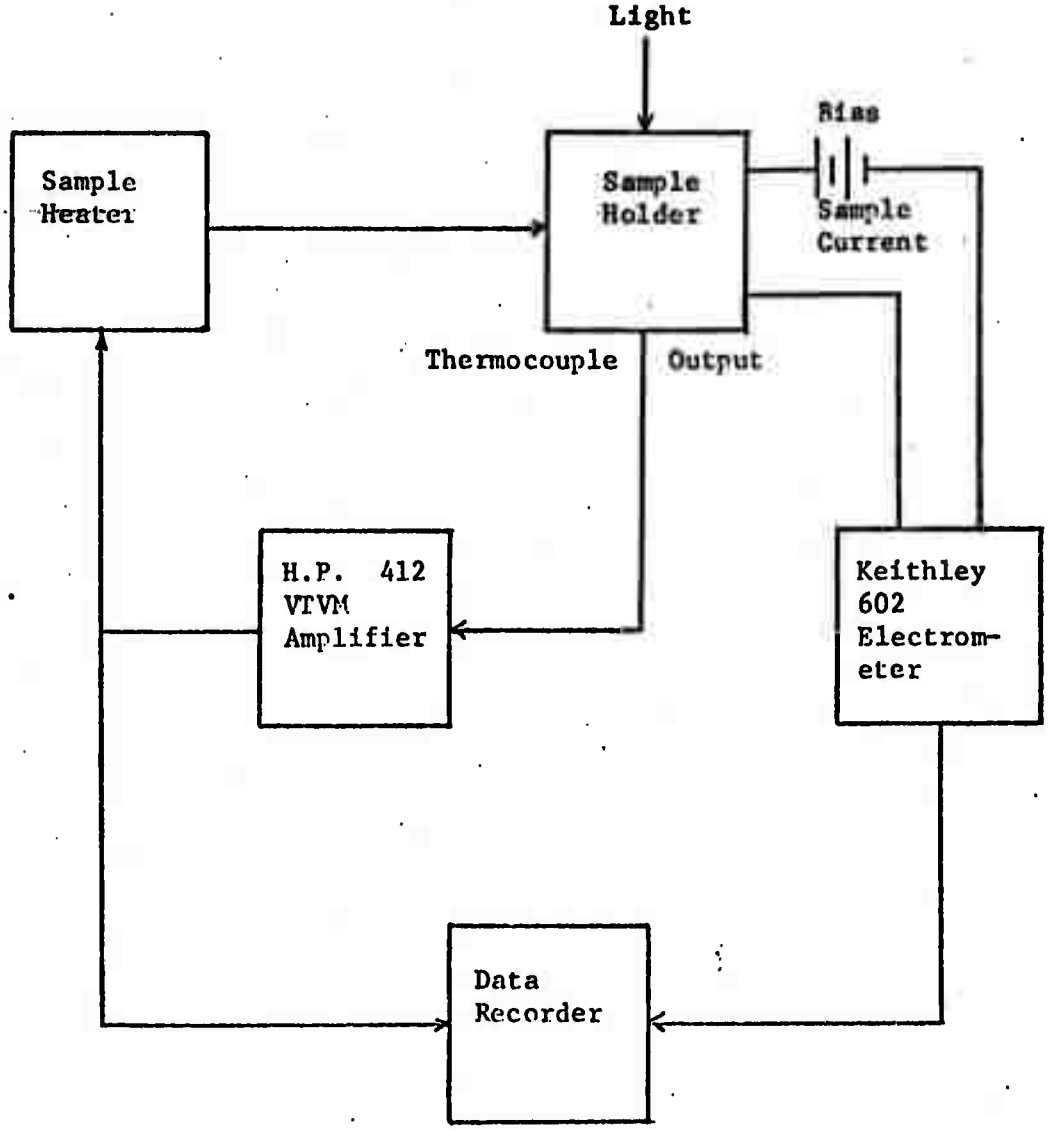

Figure II-1 Block Diagram of the TSC System Design

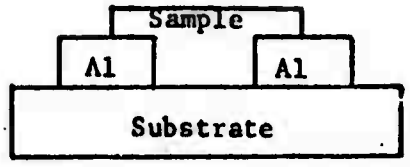

End View

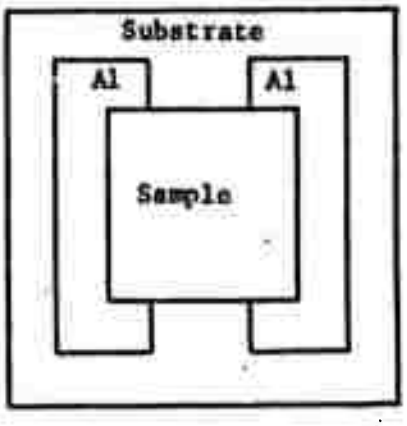

Top View

Figure II-2 Sample Geometry Used for TSC Experiment

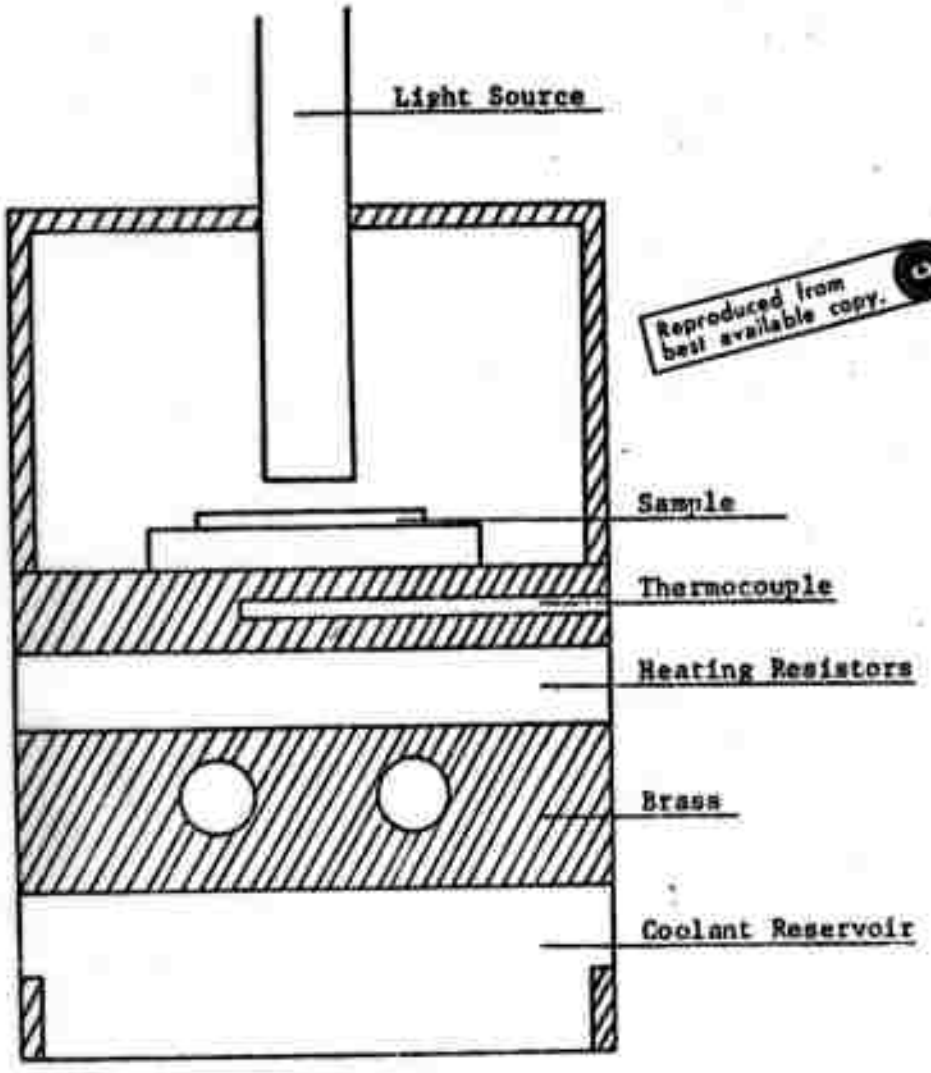

Figure II-3 Sample Holder Design (not to scale)

two watt composite resistors connected in parallel. An incandescent bulb is used to provide the necessary light which is carried to the sample by a fiber optics bundle. Leads are fastened to the aluminum contacts by an ultrasonic wire bonder using one mil aluminum wire. Coaxial cable is used to carry the signals to the ambient. The entire holder was fabricated from a single piece of brass bar stock.

Sample Heater

It was determined that a linear heating rate was needed to simplify the data analysis as much as possible. In order to determine the characteristics of the sample holder system, a cooling curve was taken (see Figure II-5). As can be seen from the curve, the system has a time constant of approximately 1.3 hours, and it is noted that a minimum of six hours is needed for the system's temperature to stabilize.

A heating curve was made using a constant input voltage for the heater supply (see Figure II-6). The curve illustrates the effect of the thermal capacitance on the system heating. In order to compensate for this effect, a feedback control system was designed to control the heater input voltage by comparing the system temperature with a predetermined reference. For a linear heating curve, the reference must approximate the voltage versus temperature curve of the chosen thermocouple (see Figure II-4 (page 75)).

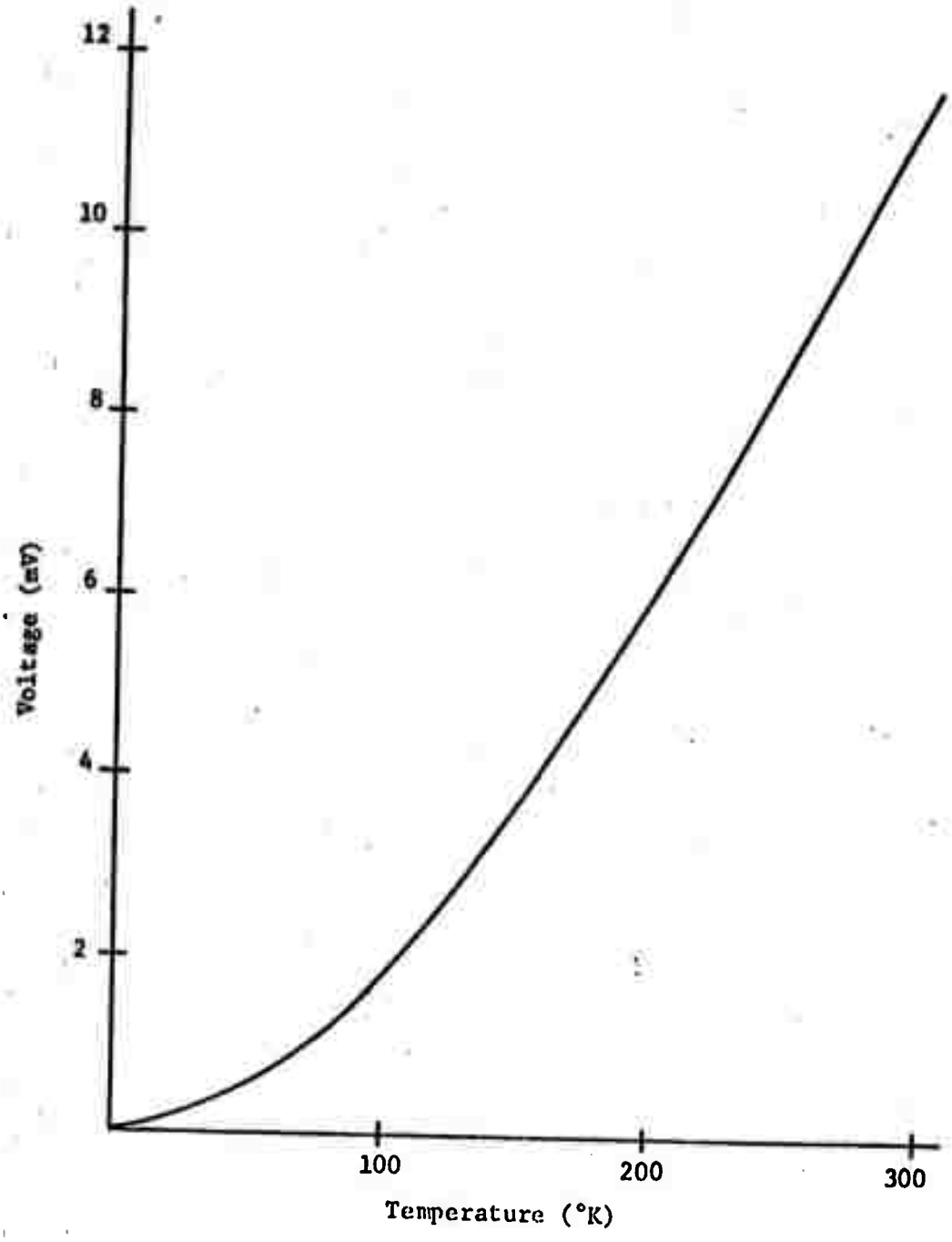

Figure II-4 Output Curve for Chromel-Constantan Thermocouple (Voltage vs. Temperature) (ref. 29)

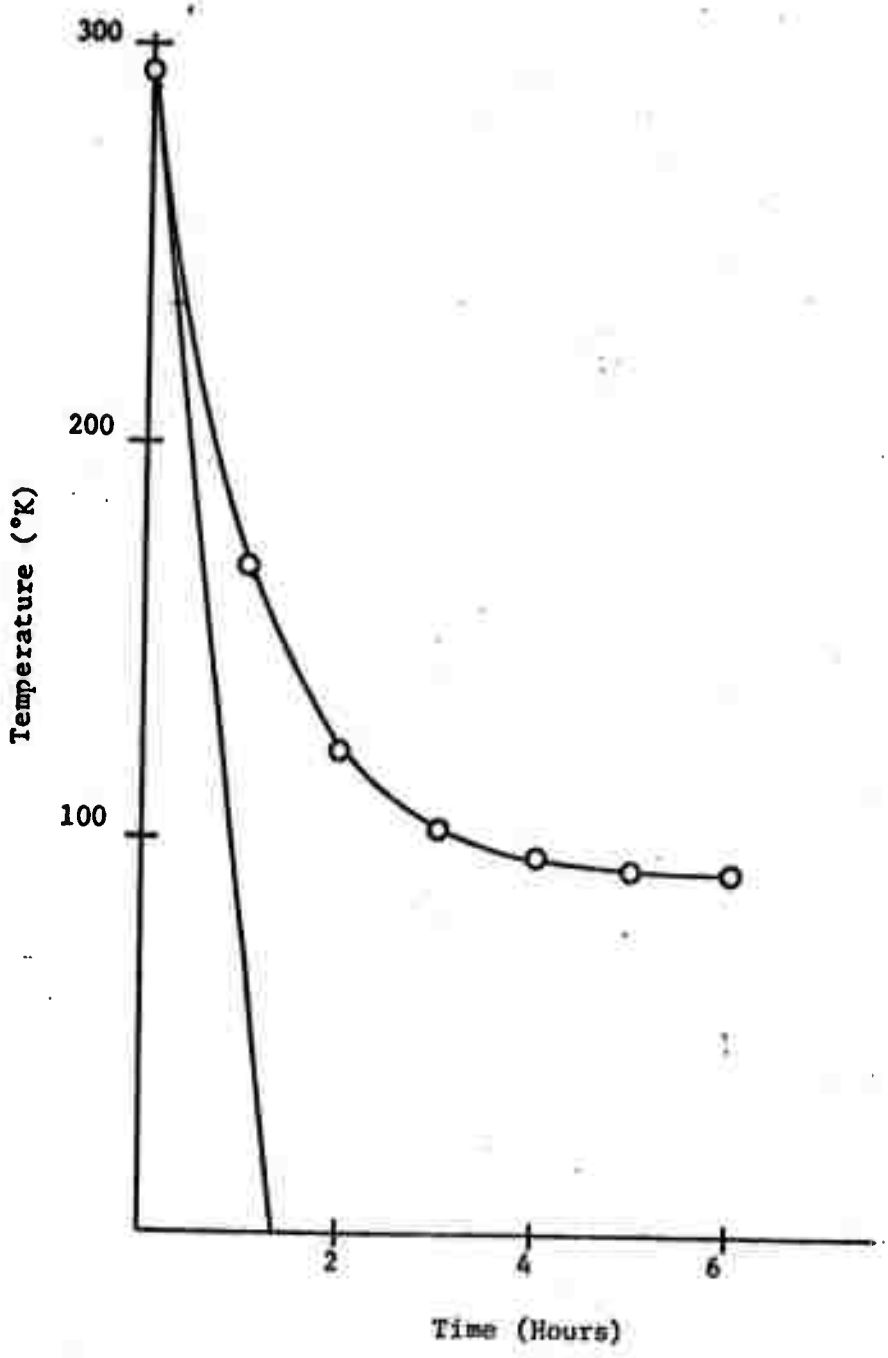

Figure II-5 System Cooling Curve (Temperature vs Time)

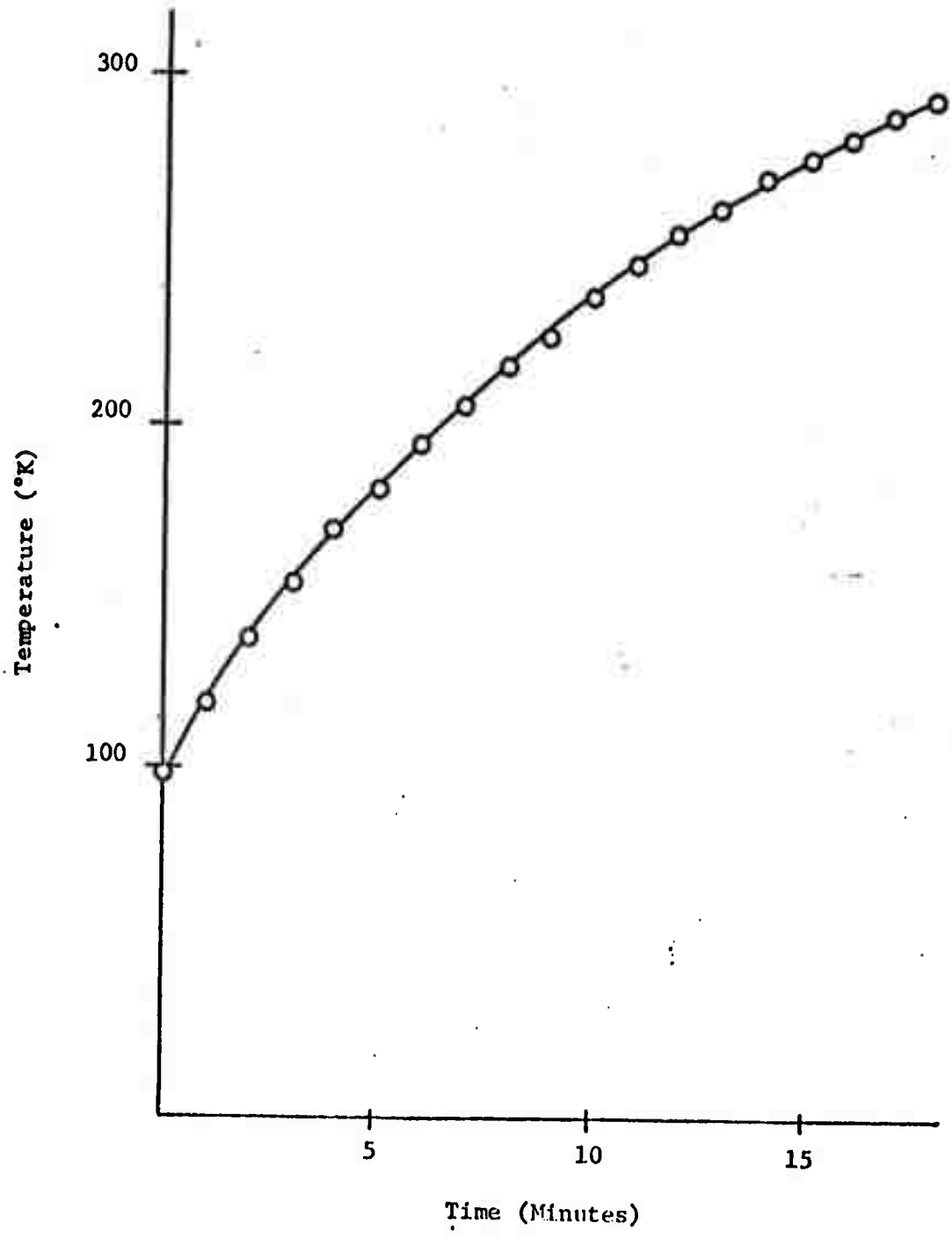

Figure II-6 System Heating Curve for a Constant Heater Voltage (Temperature vs. Time)

Two regions of temperature for As_2Se_3 were of particular interest, 100°K to 300°K, and 200°K to 450°K. As can be seen in Figure II-4 (page 75), Region I (low temperature) suggests the use of a parabolic reference voltage, and Region II (high temperature) suggests a linear or ramp reference. Two control systems were designed to effect control in these two temperature ranges.

Block diagrams of the control systems are shown in Figure II-7. (See Appendix I-A for schematic diagrams.) In control system I (Region I), a constant voltage (V_{in}) is integrated twice by operational amplifier integrators to achieve a slow rising parabolic reference voltage as shown in Figure II-8. The reference is then compared with the output voltage of the thermocouple (amplified by a H.P. 412 VTVM) by a differential amplifier which controls a Harrison 6267A programmable power supply. System heating curves using this control system for two values of V_{in} are shown in Figure II-9. Control system II is identical to control system I except that V_{in} is integrated only once to achieve a ramp reference.

Data Recorder

Several methods of recording the output data of the experiment were considered. There are two independent data outputs (temperature and sample current) which have to be correlated. It was decided to record the data digitally using two E.A.I. 5001

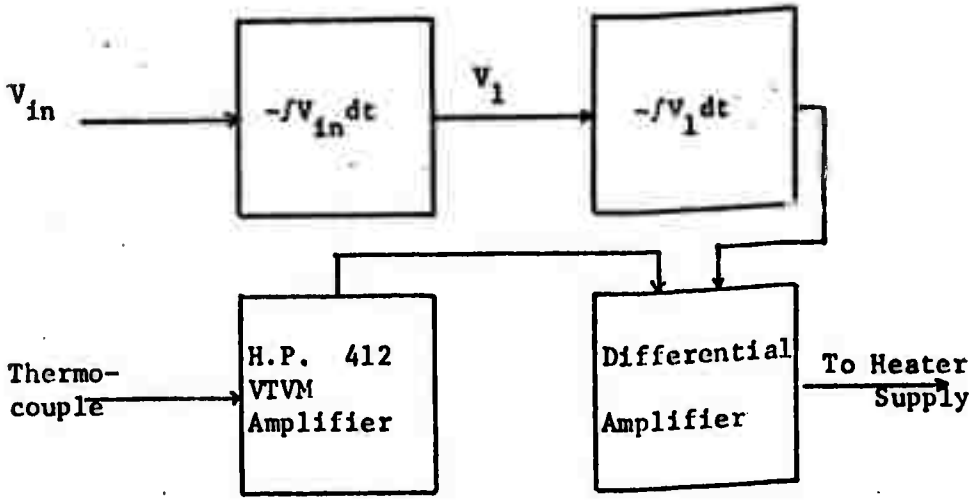

(Control System I)

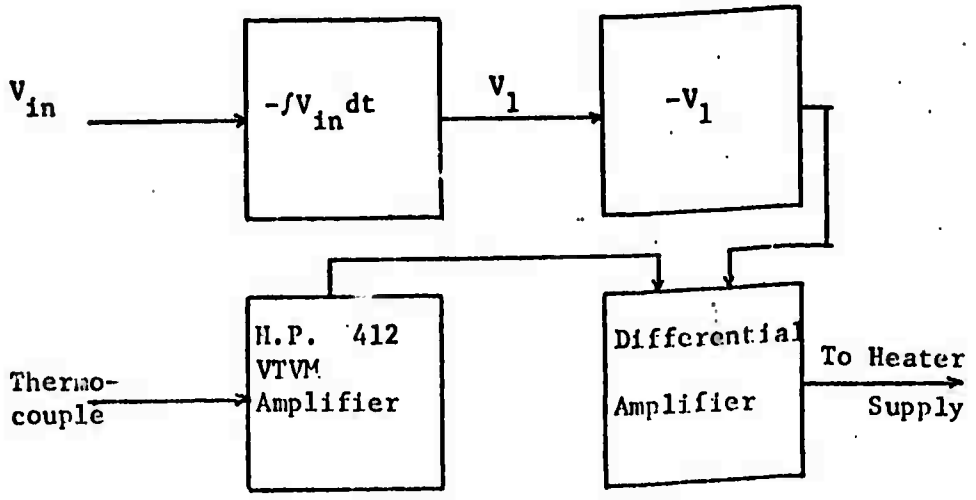

(Control System II)

Figure II-7 Block Diagrams of the Temperature Control Systems

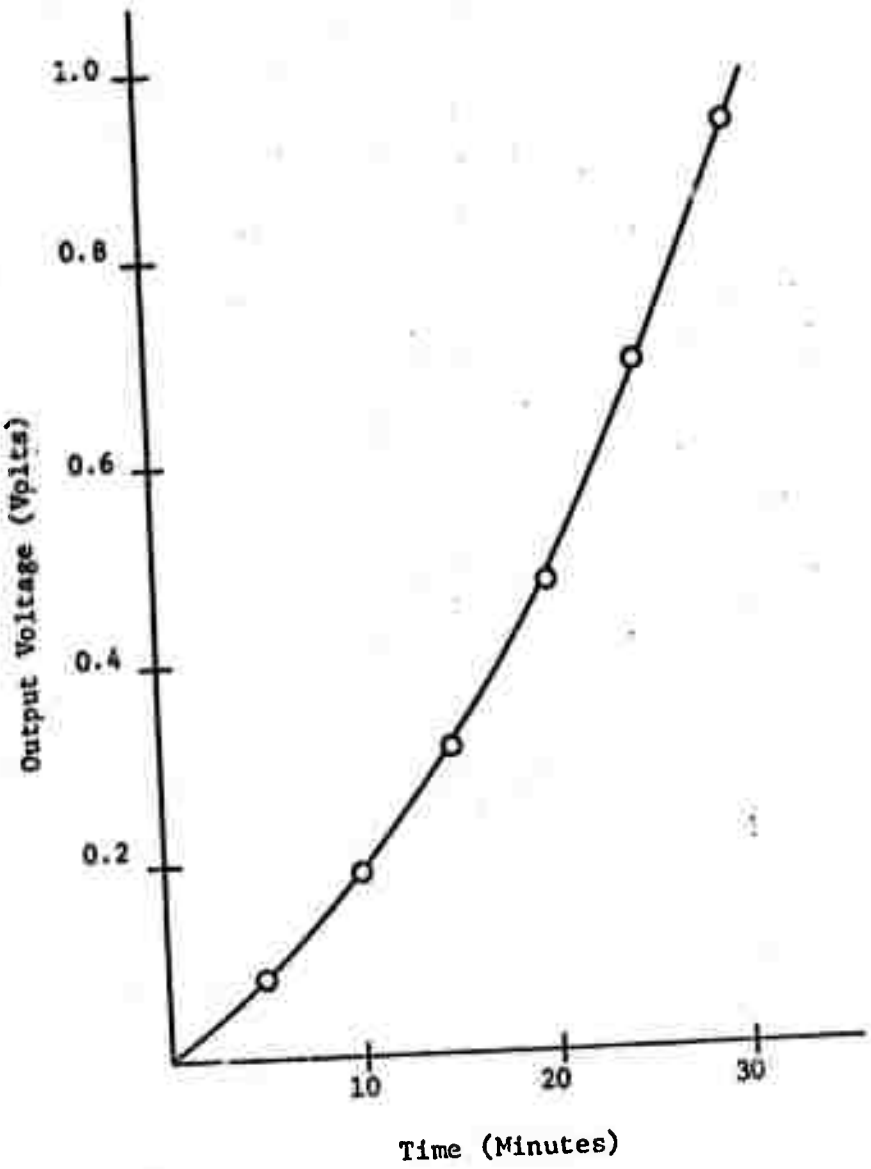

Figure II-8 Parabolic Reference Voltage (Voltage vs. Time)

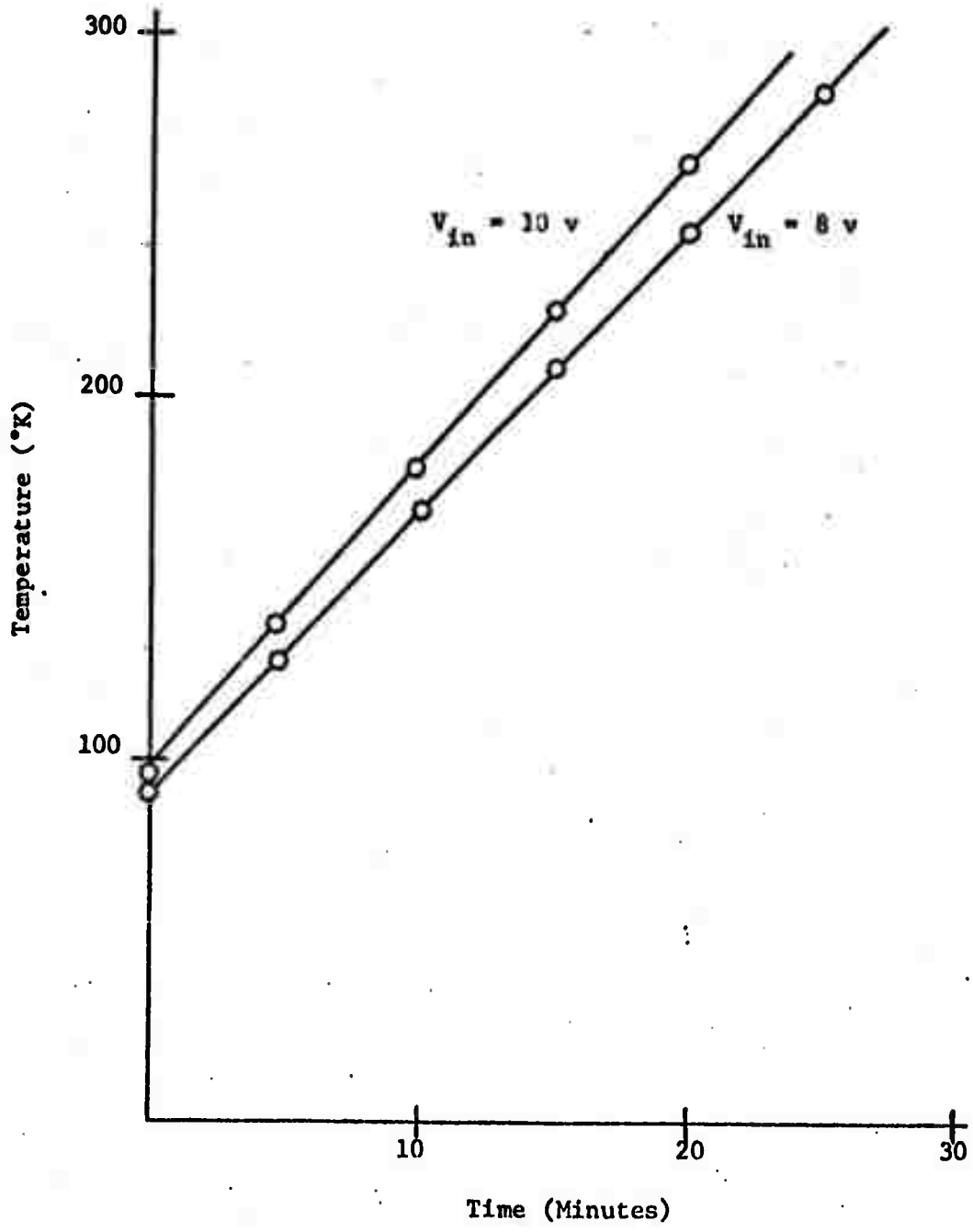

Figure II-9 System Heating Curves Using the Heater Control System (Temperature vs. Time)

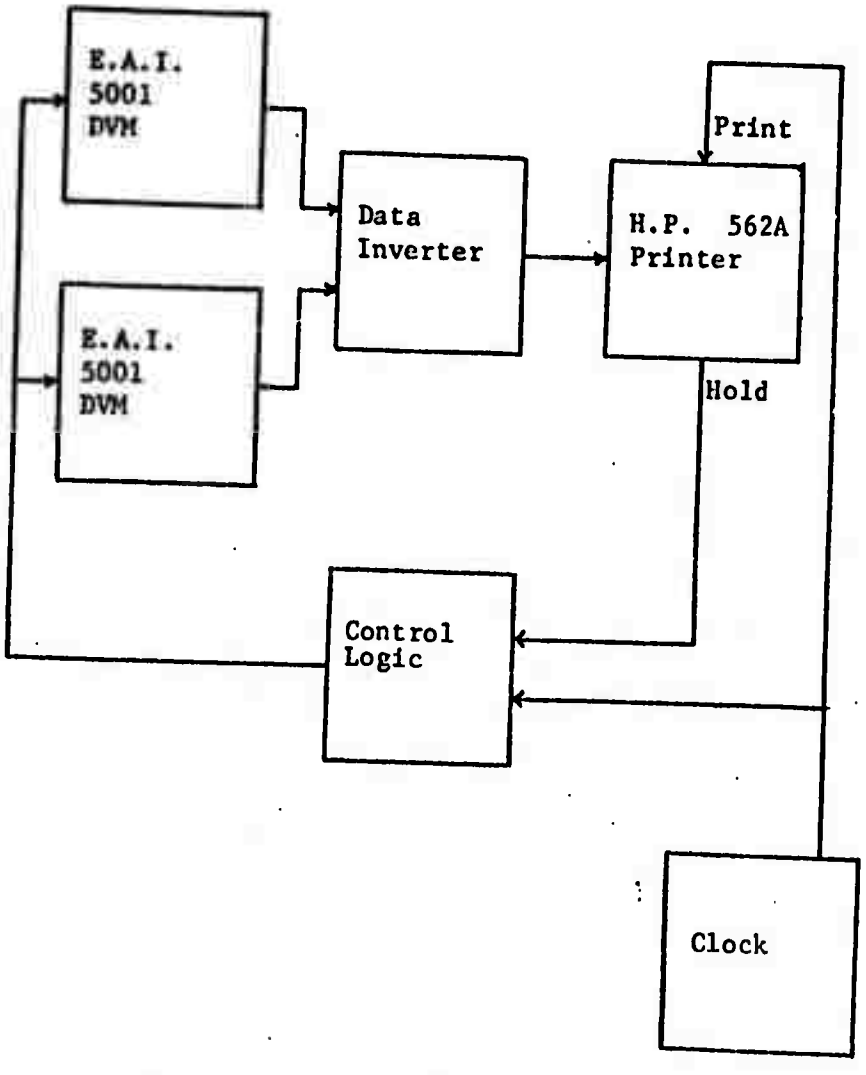

Figure II--10 Block Diagram of the Data Recording System

digital voltmeters and an H.P. 562A digital printer. Figure II-10 is a block diagram of the circuit used to correlate the meters and control the printer (see Appendix I-B for schematic diagrams). The system temperature is recorded at the output of the H.P. 412 VTVM, and the sample current is recorded at the output of the Keithley 602 electrometer (see Figure II-1 (page 71)). The printing frequency was arbitrarily chosen to be 0.5 Hertz.

Experimental Techniques

Preparation of Sample

The samples were prepared on Corning cover glass substrates using the procedures given in Appendix II. After initial cleaning (see Appendix II-A), the substrates were placed into a medium vacuum system (2×10^{-6} Torr), and aluminum was evaporated onto the substrates. The substrates were then annealed for four hours at 200°C to insure good adhesion of the aluminum, and contact patterns were subsequently etched into the aluminum by photolithographic techniques (see Appendix II-B). The substrates were then loaded into a second medium vacuum system and commercially prepared As_2Se_3 (Ventron, Alfa Inorganics Co.) was evaporated onto the contact patterns at a pressure of 5×10^{-6} Torr using a mechanical mask. Film thicknesses were on the order of 3680 Å as determined by a standard interferometric method, and the cross sectional area was 2.06×10^{-6} cm^2. The sample was then mounted into the sample holder, leads were

attached, and the system was placed into the Dewar for cooling.

Experimental Procedure

Low temperature. After the initial cooling period (approximately six hours), the sample was biased (V = 30 v), and linearly heated to room temperature in the dark by the system heater using control system I. The sample dark current was monitored by a Keithley 602 electrometer, and the temperature and current were simultaneously recorded by the digital printer. When the sample reached room temperature, the heater was turned off, and the sample was again allowed to cool. After cooling, the light was switched on, and the sample current was again monitored. When the current reached a new equilibrium value (after two to three hours), the heating cycle was repeated.

High temperature. The high temperature experiment proceeded exactly as the low temperature experiment above except that control system II was used in the system heater, and the sample was heated to 450°K.

CHAPTER III

RESULTS AND CONCLUSIONS

Results

Electron microscopy studies showed that As_2Se_3 thin films made in this manner were amorphous[30]. The constants needed for evaluation of the various equations include T, T_t, μ (the carrier mobility), m* (the effective mass), and N_c. T was taken as 7×10^{-4} sec[31], T_t as 6×10^{-3} sec[14], μ as 10 $cm^2/V\text{-sec}$[15], and m* as 2.9 x m (the carrier rest mass)[13]. N_c can be calculated from the equation:

$$N_c = 2\left\{\frac{2\pi m^* kT}{h^2}\right\}^{3/2} \qquad \text{(ref. 32)} \qquad \text{(III-1)}$$

or $N_c = 1.24 \times 10^{20}\ cm^{-3}$

where h is Planck's constant.

A graph depicting the dark conductivity (σ) versus temperature curve for As_2Se_3 at a 30 volt bias is shown in Figure III-1. There was found to be no substantial change in the conductivity at a bias of 500 volts which indicates that field effects can be ignored. Upon initial heating, the conductivity follows (I) on the plot. At a temperature of approximately 385°K, the material goes through a transformation ((II) on the plot), and with continued heating, the material follows (III) on upward. Upon subsequent cooling and reheating the material follows (IV). A plot of conductivity versus

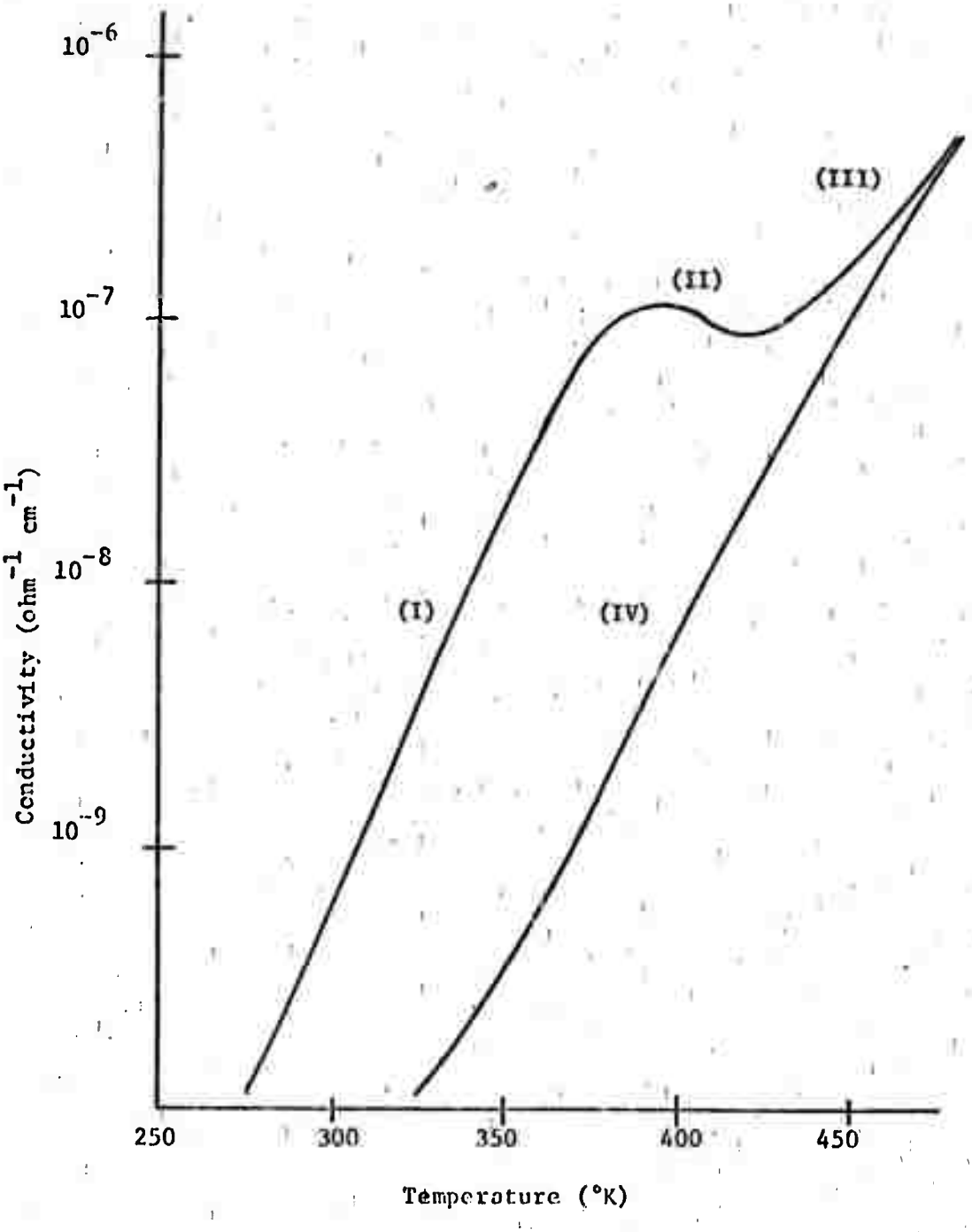

Figure III-1 Dark Conductivity of As_2Se_3 as Function of Temperature for Bias of 30 v (Conductivity vs. Temperature)

T^{-1} for (I) and (IV) is shown in Figure III-2. It may be noted that the slopes of the two curves are different which indicates that the "band gap" had changed during the transformation.

The value of the bandgap is calculated from the curves of σ versus T^{-1} by using the equation:

$$Eg = -2k \frac{d(\text{Log}_e \sigma)}{d\,(T^{-1})} \qquad \text{(ref. 33)} \qquad \text{(III-2)}$$

where E_g is the value of the bandgap. Calculations made on the curves in Figure III-2 (page 88) indicate:

E_g = 1.35 eV (Region (I))

E_g = 1.71 eV (Region (IV))

Due to the extreme instability of the photon excited material after the transformation (Region (IV)), only samples which had not been transformed were considered for further study.

A plot of the conductivity versus T for the TSC experiment is shown in Figure III-3. Three curves are shown, the conductivity in the dark, the conductivity after irradiation by light, and the thermally stimulated conductivity (the difference of the other two). It may be noted that the TSC exhibits only one peak (at T = 380°K), just prior to the transformation. The TSC was negligible below 275°K which indicates that there are no shallow traps in this material. A plot of carrier concentration (n_c) versus temperature for the TSC is shown in Figure III-4 for three different samples of As_2Se_3. This plot may be derived from the TSC by making use of the equation:

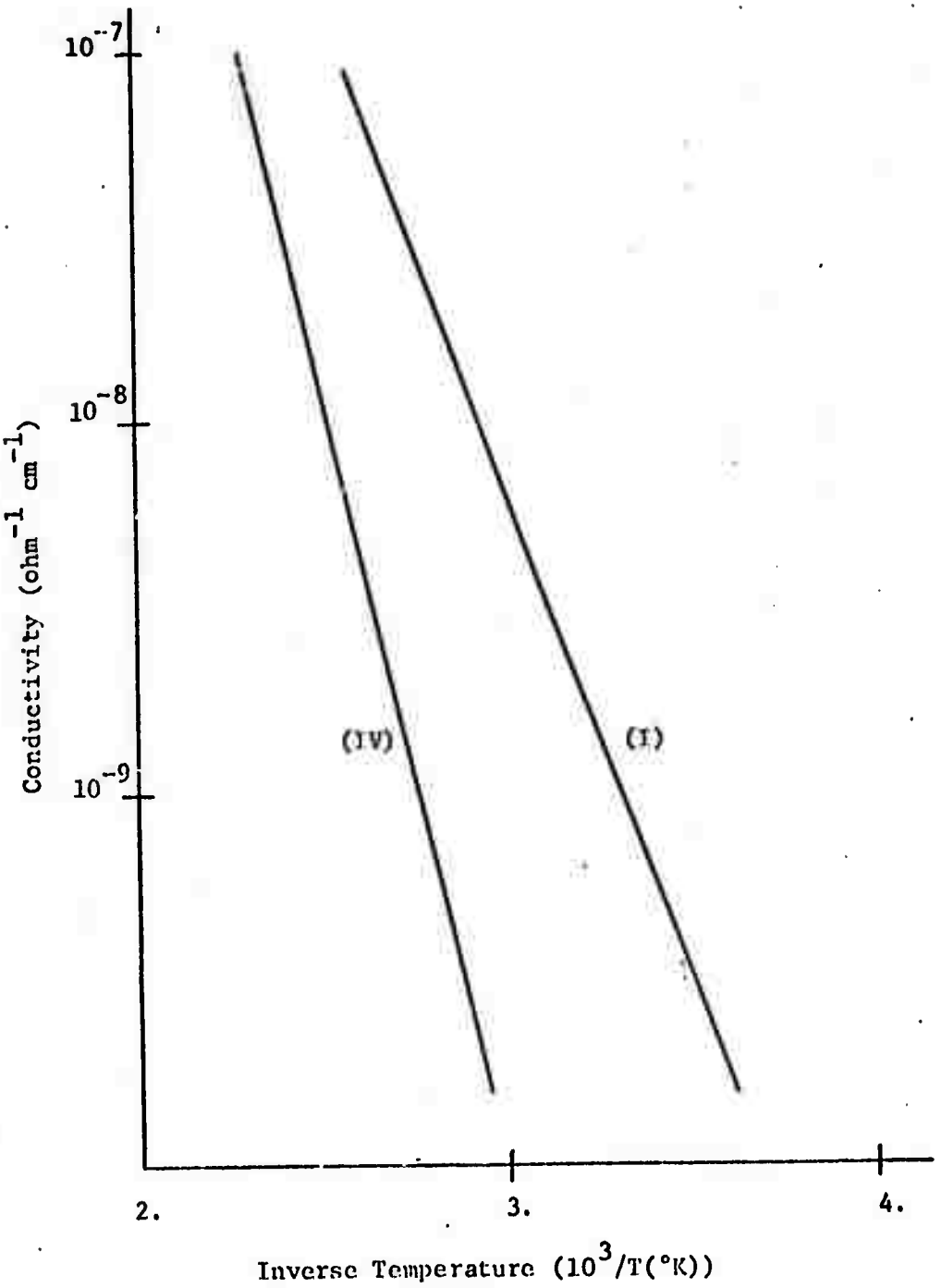

Figure III-2 Dark Conductivity of As_2Se_3 as Function of Inverse Temperature (Conductivity vs. 10^3/Temperature)

$$n_c = \frac{\sigma}{\mu e} \quad \text{(by definition)} \qquad \text{(III-3)}$$

where e is the electronic charge.

An attempt was made to analyze the observed data for both the discrete case (Equation (I-3)) and for the quasi-continuous case (Equation (I-25)). However, Equation (I-25) yielded completely unrealistic results (N_t on the order of 10^{26} cm^{-3}). There are two possible explanations for this anomaly. If the density of states in the forbidden region is discrete, Equation (I-25) breaks down because the assumption of continuity of states was the basis for the derivation. On the other hand, the density of continuous states in the forbidden region may be smaller than that postulated by the CFO model. For this case, T_t would not be constant as implied by the CFO model, but rather could vary over a wide range of values (e.g. $T_t \to \infty$ as $N_t \to 0$). Thus a suitable functional relationship between T_t and N_t would have to be determined. The former explanation is favored since the shape of the TSC curve of Figure III-3 (page 90) is quite similar to TSC curves for materials possessing known discrete trapping levels[27]. Thus, the trapping levels may be discrete or quasi-discrete, and the existence of only one peak indicates that there is only one trapping level in the material.

The energy depth of this level may be found by Equation (I-4). For the observed values of $T_m = 380°K$ and $n_{cm} = 8.5 \times 10^8$ cm^{-3}, the

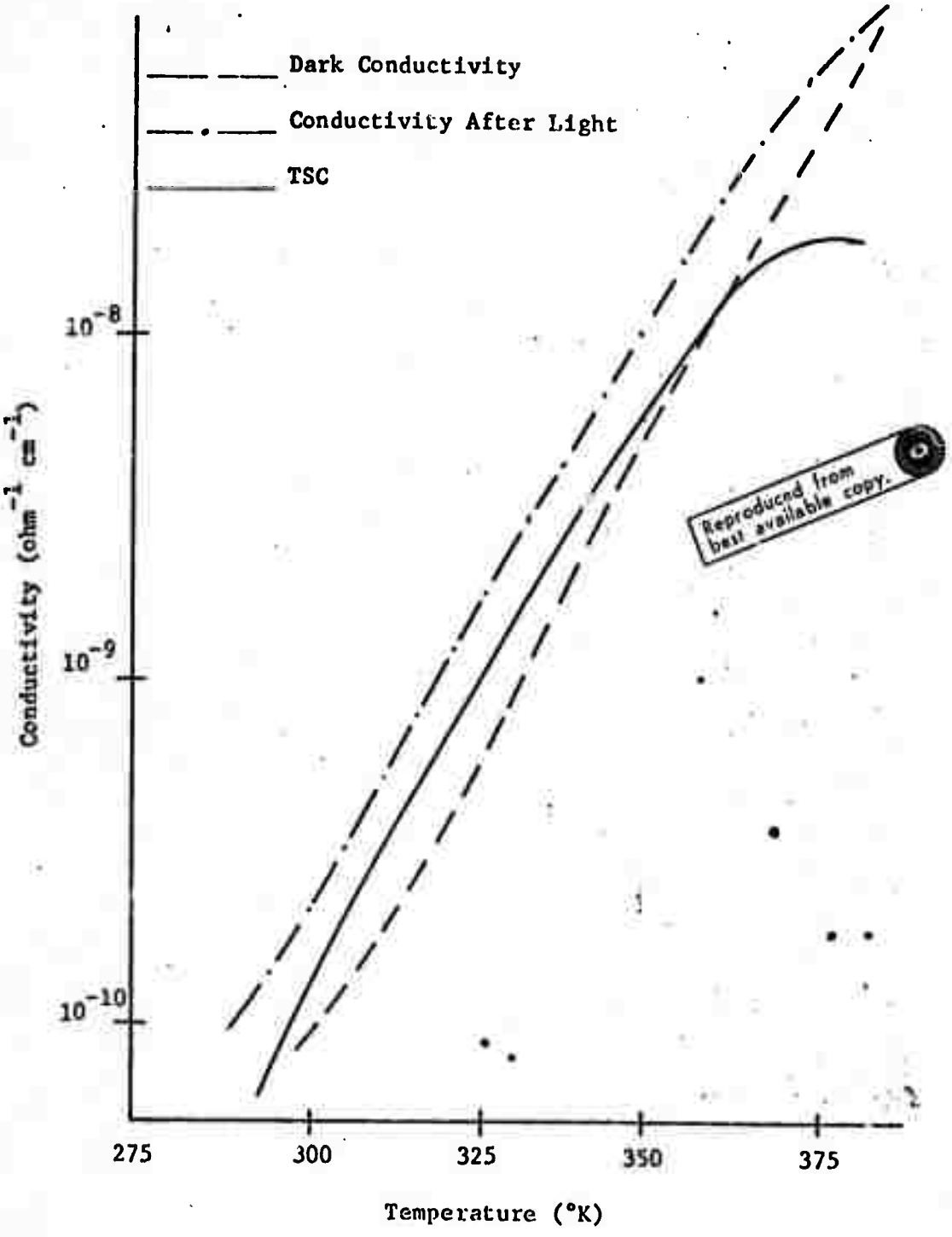

Figure III-3 Conductivity as Function of Temperature for the TSC Experiment (Conductivity vs. Temperature)

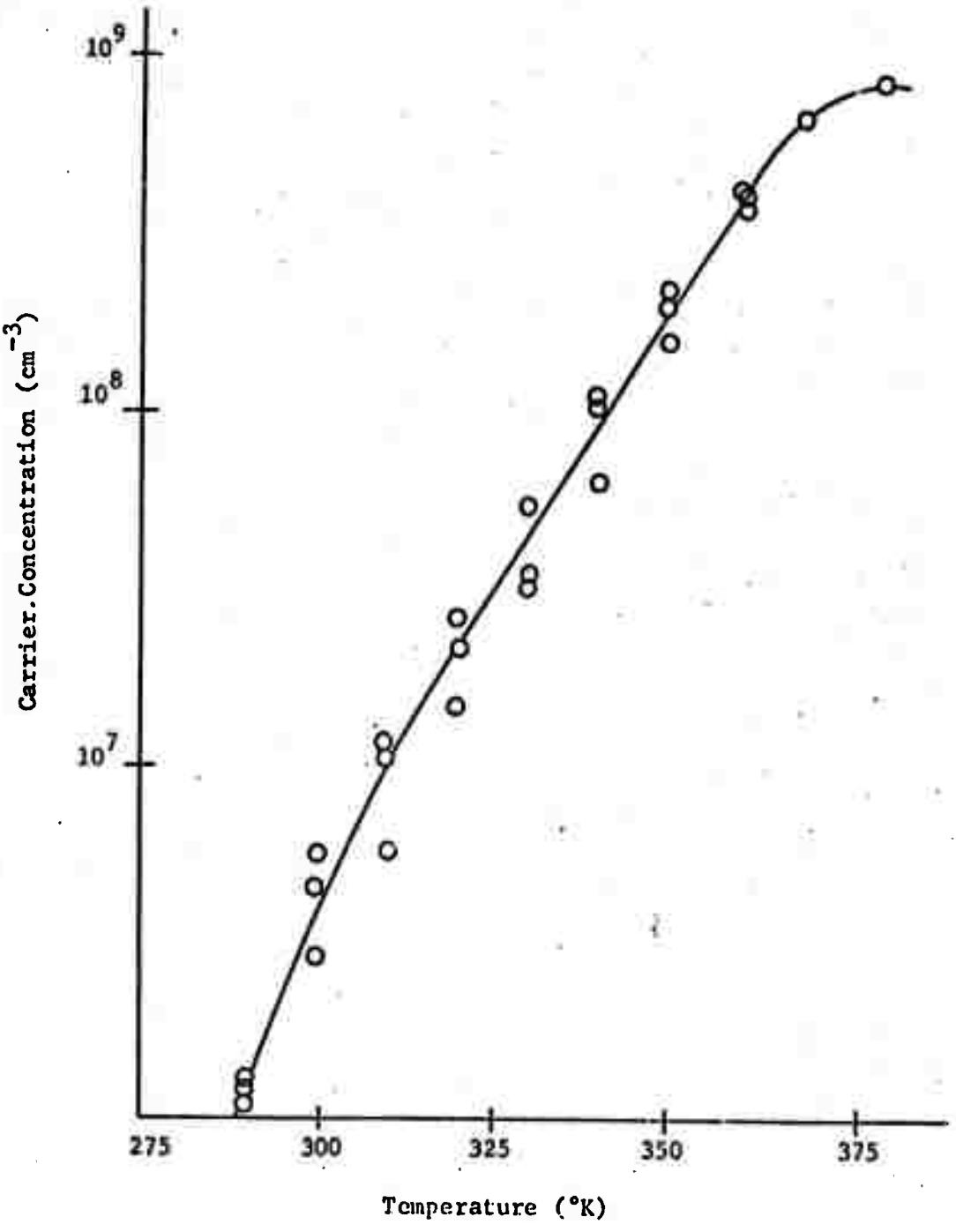

Figure III-4 Carrier Concentration as Function of Temperature for TSC (Carrier Concentration vs. Temperature)

trapping level is found to be:

$$E_t = 0.843 \text{ eV}.$$

Then, by Equation (I-3), the density of traps may be computed:

$$N_t = 9.73 \times 10^{14} \text{ cm}^{-3}.$$

The thermal velocity (ν) of the carriers may be found by using the equation:

$$\nu = \{\frac{2kT}{m^*}\}1/2 \qquad \text{(ref. 28)} \qquad \text{(III-4)}$$

or $\nu = 6.34 \times 10^6$ cm/sec.

The capture cross section (S_t) for the traps may be found by using the equation:

$$S_t = (N_t \nu T_t)^{-1} \qquad \text{(ref. 27)} \qquad \text{(III-5)}$$

or $S_t = 2.7 \times 10^{-18} \text{ cm}^2$.

Conclusions and Recommendations for Further Study

The calculated values of the band gap ($E_{gI} = 1.35$ eV and $E_{gIV} = 1.71$ eV) may be compared with reported values of 1.8-2.0 eV for As_2Se_3 in the bulk [34] and 1.7 eV for an evaporated film[31]. The change in the magnitude of the band gap indicates that the atomic structure of the material itself changed. The existence of only one discrete trapping level in amorphous As_2Se_3 indicates that the Mott-Davis model is more appropriate for this material than the CFO model. It is premature to speculate on the chalco-

genide glasses in general, but for As_2Se_3, at least, the Mott-Davis model appears applicable.

If the Mott-Davis model is assumed, since the magnitude of the trapping depth (0.843 eV) is greater than one half of the band gap (1.35/2 eV), the Fermi level must be below the middle of the gap, and thus holes are the majority carrier in amorphous As_2Se_3. Owen and Robertson[34] have measured the thermoelectric power of As_2Se_3 and have found it to be positive which also indicates that holes are the majority carriers.

In order to characterize As_2Se_3 more fully, more research is needed in several areas. The change in the magnitude of the band gap during the thermal transformation should be studied more closely. Optical experiments and electron microscopy studies might yield valuable information in this area. Expansion of the TSC experiments to include various members of the S, Se, Te family could yield trends which may give a better overall understanding of the processes involved in these materials.

REFERENCES

1) A.K. Jonscher, J. Vacuum Science and Technology 8 (1971) 135.

2) E.A. Davis and R.F. Shaw, J. Non-Crystalline Solids 2 (1970) 406.

3) J.T. Edmond, Brit. J. Appl. Phys. 17 (1966) 979.

4) K.W. Boer, J. Non-Crystalline Solids 2 (1970) 444.

5) R.S. Allgaier, J. Vacuum Science and Technology 8 (1971) 113.

6) E.A. Stern, Phys. Rev. 4 (1971) 342.

7) M.H. Cohen, E.N. Economou, S. Kirkpatrick, and T.P. Eggarter, Phys. Rev. Letters 25 (1970) 520.

8) M.H. Cohen, H. Fritzsche, and S.R. Ovshinsky, Phys. Rev. Letters 22 (1969) 1065.

9) M.H. Cohen and E.N. Economou, Mat. Res. Bull. 5 (1970) 577.

10) H. Fritzsche and S.R. Ovshinsky, J. Non-Crystalline Solids 2 (1970) 393.

11) M.H. Cohen, J. Non-Crystalline Solids 2 (1970) 432.

12) M.H. Cohen, J. Non-Crystalline Solids 4 (1970) 391.

13) N.F. Mott and E.A. Davis, Electronic Processes in Non-crystalline Materials (Oxford University Press, London, 1971).

14) B.T. Kolomiets and E.A. Lebedev, Soviet Physics-Semiconductors 1 (1967) 678.

15) B.T. Kolomiets and T.F. Mazets, J. Non-Crystalline Solids 3 (1970) 46.

16) J.T. Randall and M.H.F. Wilkins, Proc. Roy. Soc. 184A (1945) 365.

17) P.S. Pickard and M.V. Davis, J. Appl. Phys. 41 (1970) 2636.

18) G.F.J. Garlick and A.F. Gibson, Proc. Phys. Soc. 60 (1948) 574.

19) R.H. Bube, J. Chem. Phys. 23 (1955) 18.

20) W. Hoogenstraaten, Philips Res. Rep. 13 (1958) 515.

21) R.R. Haering and E.A. Adams, Phys. Rev. 117 (1960) 451.

22) P.N. Keating, Proc. Phys. Soc. 78 (1961) 1408.

23) A. Halperin and A.A. Braner, Phys. Rev. 117 (1960) 408.

24) L.F. Grossweiner, J. Appl. Phys. 24 (1953) 1306.

25) C.B. Luschik, Dokl. Akad. Nauk. SSSR 101 (1955) 641.

26) G.A. Dussel and R.H. Bube, Phys. Rev. 155 (1967) 764.

27) M.E. Haine and R.E. Carley-Read, Brit. J. Appl. Phys. J. of Phy. D. Series 2 1 (1968) 1257.

28) R.H. Bube, Photoconductivity of Solids (Wiley, New York, 1960).

29) L.L. Sparks, R.L. Powell, and W.J. Hall, NBS Report 9712, National Bureau of Standards.

30) J.L. Barrett, Texas A&M U., Unpublished.

31) B.T. Kolomiets and V.M. Lyubin, Soviet Physics-Solid State 4 (1962) 291.

32) A. van der Ziel, Solid State Physical Electronics (Prentice Hall, Englewood Cliffs, N.J., 1968).

33) R.L. Ramey, Physical Electronics (Wadsworth, Belmont, Ca., 1961).

34) A.E. Owen and J.M. Robertson, J. Non-Crystalline Solids 2 (1970) 40.

APPENDIX I

SCHEMATIC DIAGRAMS

I-A Temperature Control Systems

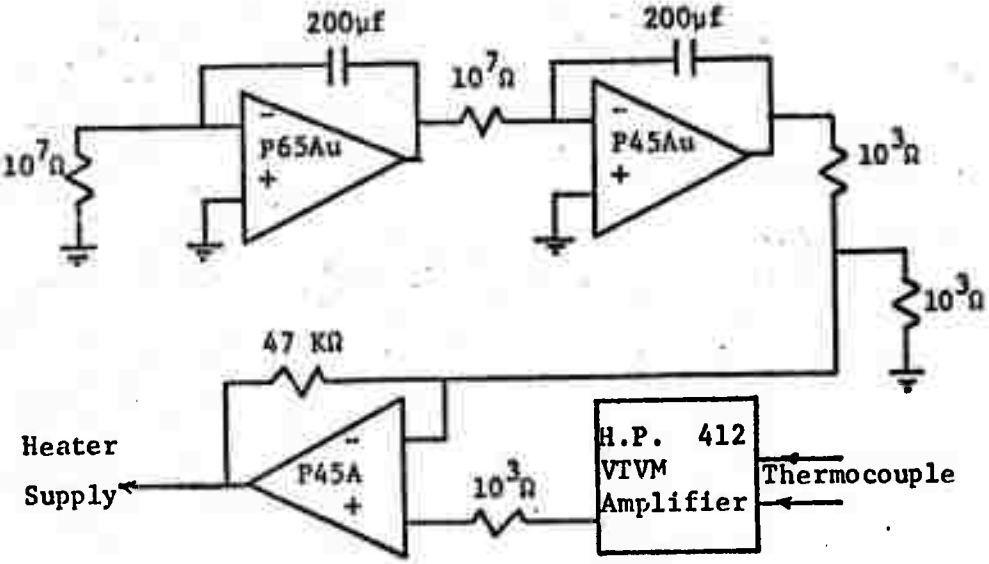

(Control System I)

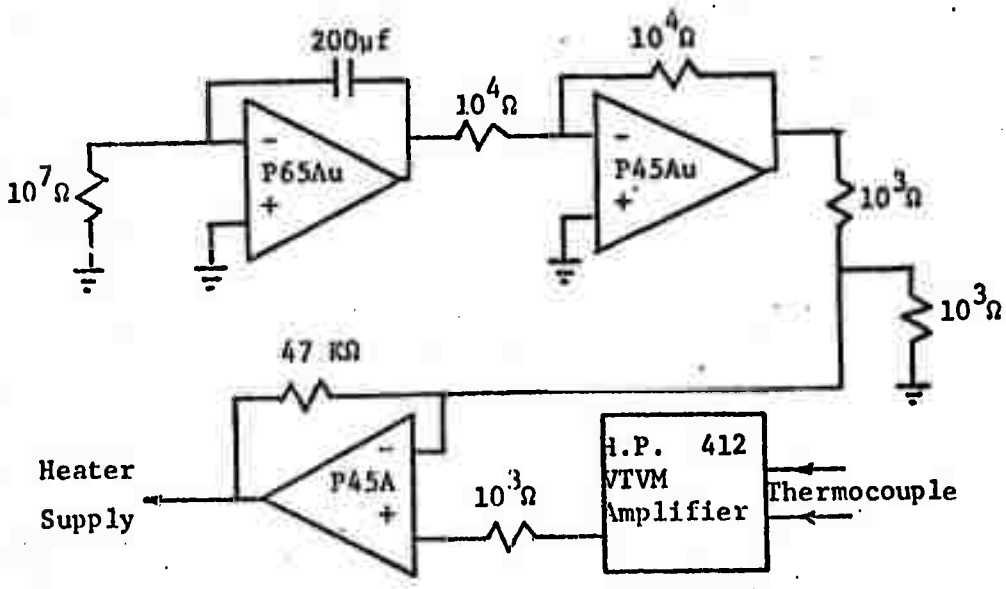

(Control System II)

I-B Printer Interface

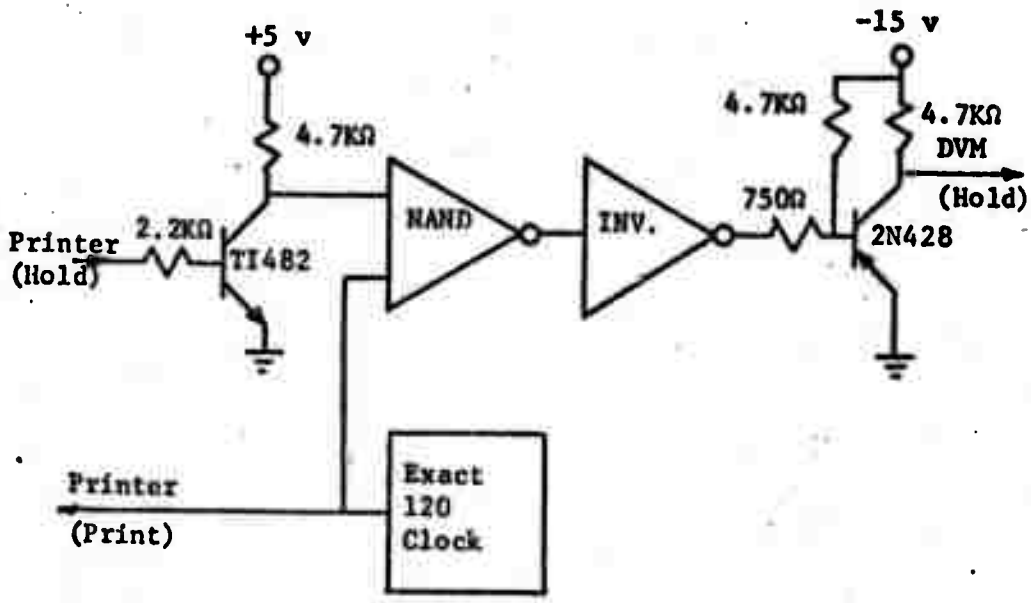

(Print Control Logic)

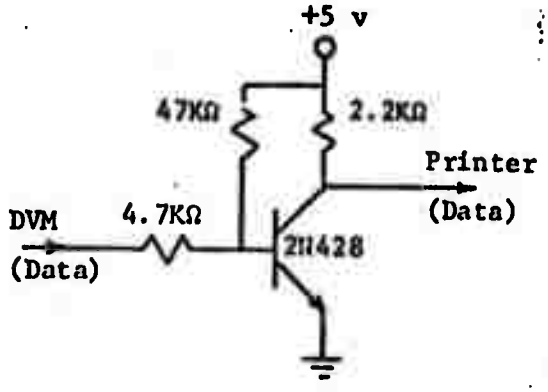

(Data Inverter (DVM to Printer)

APPENDIX II

EXPLRIMENTAL PROCEDURES

II-A Initial Cleaning

The substrates are placed in a quartz jig and cleaned by the following procedure. Note: Steps 1-6 are carried out in an ultrasonic cleaner.

(1) 5 minutes in Microclean commercial glass cleaner at 100°C.

(2) 5 minutes in deionized water at 100°C.

(3) 5 minutes in deionized water at 100°C,

(4) 5 minutes in deionized water at 100°C.

(5) 5 minutes in boiling 2-propanol.

(6) 5 minutes in boiling 2-propanol.

(7) Dry under dry nitrogen.

II-B Photolithographic Procedure

(1) 5 minutes in boiling 2-propanol.

(2) Bake in oven for 5 minutes at 100°C.

(3) Apply KMER-33, spinning at 4000 rpm for 30 sec.

(4) Bake for 10 minutes at 100°C.

(5) Expose in mask aligner for 15 sec.

(6) Develop in xylene for 3 minutes.

(7) Wash in 2-propanol for 3 minutes.

(8) Slow rise on slowrise plate to 180°C.

(9) Etch in aluminum etch.

(10) (KMER strip) 5 minutes in A20 strip at 90°C (±5°C).

(11) 2 minutes in boiling trichloroethylene.

(12) 2 minutes in boiling trichloroethylene.

(13) 5 minutes in boiling deionized water.

(14) 5 minutes in boiling deionized water.

(15) Dry under nitrogen.

Note: Aluminum etch formula (by volume)

85% Phosphoric acid

10% Nitric acid

5% Deionized water

APPENDIX III

OBSERVED VALUES OF TSC IN As_2Se_3

Temperature (°K)	TSC (ohm^{-1} cm^{-1})
290	3.23×10^{-11}
300	1.2×10^{-10}
310	2.89×10^{-10}
320	6.76×10^{-10}
330	1.4×10^{-9}
340	2.86×10^{-9}
350	5.75×10^{-9}
360	1.12×10^{-8}
370	1.75×10^{-8}
380	1.95×10^{-8}